A LARGE EXTENDED OPENING IN THE WEB OF A WIDE-FLANGE BEAM

AN INVESTIGATION OF LARGE EXTENDED OPENINGS IN THE WEBS OF WIDE FLANGE BEAMS

by

Shih-yuan Cheng

A thesis submitted to the Faculty of Graduate Studies and Research in partial fulfilment of the requirements for the degree of Master of Engineering

Department of Civil Engineering
McGill University, Montreal, P.Q.

August, 1966

ACKNOWLEDGEMENTS

The author wishes to express his deep appreciation to those who so kindly provided assistance during the course of this project. Special thanks are due to:

Professor J.O. McCutcheon, who acted as Research Director and provided valuable advice and guidance during the course of the investigation;

Dr. R.G. Redwood, who gave valuable suggestions in the development of the theories and during the preparation of this thesis;

Dr. J.F. Dickie, who provided valuable assistance during the course of the experiments, especially the photostress technique;

Messrs. G. Matsell, W. Lambert and P. McGrath, laboratory technicians, who gave generous help in carrying out the tests.

This investigation was made possible by the financial assistance of the Canadian Institute of Steel Construction and forms part of a general study of beam behaviour with various web openings supported by the Canadian Institute of Steel Construction.

SUMMARY

The elastic and plastic behaviour of a wide-flange beam with a large extended opening in the web is investigated theoretically and experimentally for various loading conditions.

Two different methods are introduced for calculating the elastic stresses at the boundary of the opening for pure bending and for pure shear. One is the "small hole theory" based on the theory of elasticity assuming that the dimensions of the opening are small compared with the depth of the beam. The other is an approximate method treating the beam near the opening as an elastic ring. The stresses for the case of bending with shear are calculated by superposition.

The ultimate strength of the beam is analyzed and three solutions are developed which apply to loadings of pure bending, bending with a small amount of shear and bending with large shear, respectively. Equilibrium is satisfied in each case by considering shear, axial force and moment force at each yield position.

Experiments are described in which two specimens of A36 steel 14" at 30 lb wide-flange beams each with a single extended opening were tested under four shear to moment ratios. Measurements of deflections and elastic strains under different loading conditions and at various stages of loading were recorded and also the ultimate strength of the beams.

The theoretical values are compared with the experimental results both for elastic stresses and for the ultimate strength. The

agreement between the measured and predicted elastic stresses is satisfactory for practical design application. The general validity of the ultimate strength solutions can be established only after further experimental investigation.

NOTATION

The following notation is used in this thesis unless explicitly stated otherwise:

A,B,C,D,E	Real coefficients of mapping function
A_t	Area of the tee
A_f	Area of the flange
a	Length of rectangular portion of the opening
b	Flange width
D	Web depth of the tee
e_x	Axial unit strain
e_y	Normal unit strain
e_{xy}	Shear unit strain
e_t	Tangential unit strain at free boundary
F	Stress concentration factor
F_c	Reinforcement correction factor
H	Total depth of the beam
h	Half-height of the beam
h_c	Distance between the centroids of the upper and lower tee
I	Moment of inertia of the beam
I_n	Moment of inertia of the net section of the beam
K	Strain-optical sensitivity of plastic sheet
N_n	Fringe order in normal incidence
P	Applied load

R	Reaction force
r	Radius of half circle portion of the opening
t_f	Flange thickness
t_p	Thickness of plastic sheet
t_w	Web thickness
Y_f	Yield point stress of the flange
Y_w	Yield point stress of the web
$\bar{y}$	Distance from the boundary of the opening to the centroid of the tee
y_o	Half-height of opening (= A - B + C - D + E)
Z	Section modulus of the beam
σ_{max}	Maximum stress
σ_{nom}	Nominal stress
σ_t	Tangential stress at boundary of opening
σ_x	Axial (or direct) stress
σ_y	Normal stress
$\sigma_{y.p.}$	Yield point stress in tension
τ_{xy}	Shear stress
$\tau_{y.p.}$	Yield point stress in shear
λ	Wave length of light corresponding to the retardation at the tint of passage (22.7×10^{-6} inches)
μ_s	Poisson's ratio of sample beam
(α, β)	Orthogonal curvilinear coordinates
Γ	Shear parameter, a measure of maximum shear stress in the web

TABLE OF CONTENTS

CHAPTER I

INTRODUCTION

In steel building structures, it is frequently required to have openings in the webs of the beams for the passage of electrical and mechanical services. Sometimes these openings are more than half of the depth of the beam web, and their effects on the elastic and plastic behaviour of the beam are not yet completely understood. Reinforcement of these openings is usually expensive, and it is the purpose of this investigation to study a particular shape of unreinforced opening in an attempt to determine the conditions when reinforcement is not necessary.

The behaviour of a large extended (ovaloid) opening with parallel sides ended by two semi-circles (Figure 2-2a), in the web of a wide-flange beam will be analyzed theoretically and experimentally for different loading conditions.

1.1 HISTORICAL REVIEW

1. Elastic Stresses

Since the end of the last century, a lot of work has been done concerning the stress concentration around an opening in a plate. Most of the earlier efforts were concerned with a circular opening in an infinite plate, in an infinite strip, and in a finite plate. The stress distribution around a circular hole in an infinite plate under

tension was solved by Kirsch in 1898[1], and that under pure bending by Tuzi in 1928[2]. These solutions are applicable to the case of an infinite strip if the ratio of the hole diameter to the plate width is respectively less than 0.25 for simple tension[3] and 0.6 for pure bending[2]. An infinite strip, containing a symmetrically located circular opening, with its diameter up to 50% of the plate width, was analyzed for simple tension, pure bending and bending with shear by Howland and Stevenson[4] in 1933, using a method of successive approximation. This same strip under tension was investigated by Knight[5] in 1934 in a way which is more direct than that used by Howland. In an extension of the methods of Howland[4] and Hengst[6], Wang[7] published a paper in 1946 which dealt with an infinite strip and a finite plate containing a symmetrically located circular hole under pure shear. A different solution for an infinite strip containing an unsymmetrically located circular opening under simple tension and pure bending was presented by Lin[8] in 1957. All this above mentioned work deals with a plate of rectangular sections. Large circular openings in a plate which forms the web of a wide-flange beam have recently been investigated by Gibson and Jenkins[9] and So[10] for a number of different loading conditions.

Much work has also been done on an infinite plate with a non-circular opening: Kolosoff[11] and Inglis[12] first investigated the elliptical hole under simple tension. Later Wolf[13] and Neuber[14] worked on the same opening under pure bending and shear respectively. An ovaloid (extended) opening under uniform load was analyzed by

Greenspan[15], and triangular and rectangular holes by Green[16]. All these solutions are for a hole in an infinite plate, and have been solved by means of either real or complex variable stress functions. However, the most important work was done by Muskhelishvili[17] and his associates, who, as early as the 1930's, developed a general and direct method for determining the complex potentials by using the Cauchy integral at the boundary of the opening, without the necessity of guessing their form in advance. Following this technique, Morkovin[18], Savin[19], the group in David Taylor Model Basin[20,21,22,23] and Bower[24] solved a series of problems, concerning a small hole of various shapes in a plate or in the web of an I-beam under various loading conditions.

However, no exact solution has been worked out for an infinite strip or a finite plate containing a non-circular opening, like its counterpart, the circular hole, as done by Howland and Stevenson, Knight, Wang and Lin.

Mathematically, Muskhelishvili's method is not applicable to the case of finite plate or an infinite strip. However, for some particular loading conditions (e.g. pure bending), it does give an approximate results which is sufficiently accurate for practical application. The reason for this will be discussed in Chapter V.

A beam with a small extended opening in the web under different loading conditions was investigated by the group in David Taylor Model Basin: The solution for the case of pure bending was

presented by Joseph and Brock[20], and that for bending with shear by Heller[21]. All used a curvilinear coordinate associated with Greenspan[15]. A solution for the stresses around a small rectangular opening with round corners in the web of a beam subjected to bending with shear was presented by Heller et al.[23] in 1959, using a curvilinear coordinate different from that of Greenspan. This solution is valid for different corner radii of the opening and in particular is applicable to the case of the extended opening. The result of this solution shows an improvement on their previous work[20,21], since the new curvilinear coordinate, as determined by the new mapping function, produces a better fit to the boundary curve of the opening.

Instead of rigorous analysis based on theory of elasticity, an approximate "Vierendeel" method[25] (in the latter part of this thesis, it is referred to as ring theory) has been used to calculate the elastic stresses around rectangular holes in the web of wide-flange beams. This method is sometimes referred to as the Vierendeel method because the beam, near the holes, is assumed to act like a Vierendeel frame.

A great deal of experimental work has been done to verify the stress conditions around an opening in a plate, mostly by means of photoelasticity. Experiments on a wide-flange beam with openings of different shapes have recently been carried out by Gibson and Jenkins[9], Segner[26], McClellan[27], So[10], and Bower[28].

2. Ultimate Strength of the Beam

Little work has been done concerning the ultimate strength of a wide-flange beam with an opening in the web. In 1958 Worley[29] analyzed a beam with elliptical holes in the web by upper bound theory, neglecting the effects of shear and axial forces at the yield sections. A more rigorous analysis was recently given by Bower[30] who investigated a wide-flange beam with a rectangular opening in the web by considering the effect of shear on the yield sections. However, no axial force effect was taken into consideration in his solution, and thus the equilibrium condition is not always satisfied for a free body taken from the beam.

1.2 OBJECT AND SCOPE OF INVESTIGATION

The object of this investigation was to study theoretically and experimentally the elastic and plastic behaviour of a wide-flange beam with a large extended opening in the web subjected to pure bending and bending with shear. It was desired to establish satisfactory methods for predicting elastic stresses around the opening and the ultimate strength of the beam.

Since the exact elastic analysis for a large opening is difficult and not immediately possible, efforts were made to find an approximate solution which is accurate enough for practical design applications.

An approximate lower bound theory was developed for ultimate strength analysis. The solutions were based on the equilibrium condition of a free body bounded by two yield sections, with the shear, axial and moment forces at these sections all taken into consideration. The possible failure of the beam due to local inelastic buckling was beyond the scope of this investigation.

The experiments were performed on two 14 inch at 30 lb wide-flange beams of A36 steel. Elastic strains and the deflections of the beams were measured and also the ultimate strengths.

CHAPTER II

THEORETICAL APPROACHES - ELASTIC STRESSES

The elastic behaviour of a wide-flange beam with a large extended opening in the web is analyzed for pure bending, pure shear, and bending with shear. Two different methods are briefly introduced. One is the comparatively exact method based on theory of elasticity assuming that the dimensions of the opening are small compared with the depth of the beam. The other is an approximate method treating a length of the beam containing the opening as an elastic ring. These solutions are all based on the usual assumptions of plane elasticity: homogeneous, isotropic material within the elastic limit, and uniform stress across the thickness of the web with no stress normal to the plane of the web.

2.1 PURE BENDING

1. Small Hole Theory

Based on the complex variable method associated with Muskhelishi[17], Heller et al. have developed a theory for the case of pure bending, with the assumption that the hole is small compared with the depth of the beam. The tangential stress at the boundary of the opening can be obtained from the following formula[23]

$$J_o^2 \left(\frac{\sigma_t}{\frac{My_o}{I}}\right) = \frac{A}{y_o}(\Delta_1 \sin\beta + \Delta_3 \sin 3\beta + \Delta_5 \sin 5\beta + \Delta_7 \sin 7\beta + \Delta_9 \sin 9\beta) \quad (2\text{-}1)$$

where σ_t is the tangential stress at the boundary and

$M = \frac{PL}{2}$ (Figure 2-1)

I = moment of inertia of the wide-flange beam without any opening

y_o = half-height of opening, A - B + C - D + E

A, B, C, D, E = real coefficients of mapping function which can be found in Table D.1, Appendix D.

$\Delta_1 = A^2 - a_2'AB + 3a_2'AC - 6a_4'AC + 10a_4'AD - 30\,K_3AD + 42\,K_3AE - 56E^2$

$\Delta_3 = a_2'A^2 - AB - 2a_4'AB - 18\,K_3AC + 5a_2'AD - 40\,DE + 14a_4'AE$

$\Delta_5 = 2a_4'A^2 - 6\,K_3AB - 3AC - 24\,CE + 7a_2'AE$

$\Delta_7 = AD - 2BE$

$\Delta_9 = AE$

$J_o^2 = S_o + S_2\cos 2\beta + S_4\cos 4\beta + S_6\cos 6\beta + S_8\cos 8\beta$

$S_o = A^2 + B^2 + 9C^2 + 25D^2 + 49E^2$

$S_2 = -2(AB - 3BC - 15CD - 35DE)$

$S_4 = -2(3AC - 5BD - 21CE)$

$S_6 = -2(5AD - 7BE)$

$S_8 = -14AE$

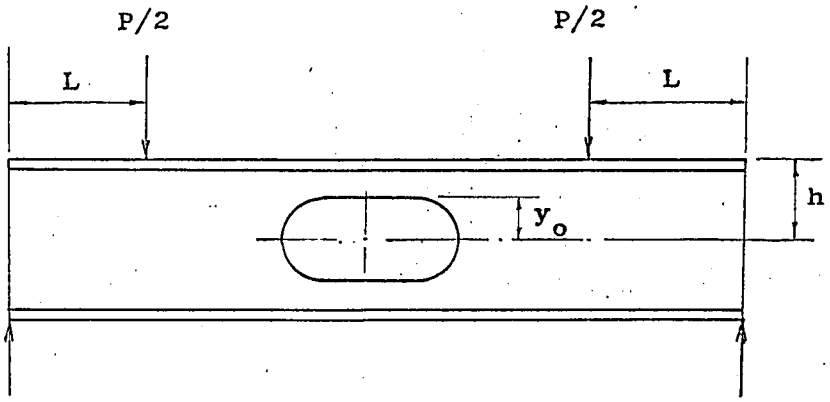

Fig. 2-1 Pure Bending Loading Condition.

$$a_2' = \frac{2K_1 - 1 - 8\,K_1K_5}{1 + 2\,K_3 - 8\,K_1^2}$$

$$a_4' = 2(\bar{K}_5 - \bar{K}_1 a_2')$$

$$K_1 = \frac{E}{A}$$

$$K_3 = \frac{D}{A} + \frac{B}{A} K_1$$

$$K_5 = \frac{C}{A} + \frac{B}{A} K_3 + \frac{3C}{A} K_1$$

$$K_7 = \frac{B}{A} + \frac{B}{A} K_5 + \frac{3C}{A} K_3 + \frac{5D}{A} K_1$$

β = one of the curvilinear coordinates defining the positions of points on the boundary of the opening.

2. Ring Theory

The structural element shown in Figure 2-2a can be considered as an elastic ring with loadings acting on both sides. This is a statically indeterminate structure with two redundant forces. However, the axial stresses on the central sections of both top and bottom members can be approximately calculated from the following formula[25], based on the assumption of the plane section remaining plane at the section concerned.

$$\sigma_x = \frac{My}{I_n} \qquad (2\text{-}2)$$

where σ_x is the axial stress on the tee section (Figure 2-2b). M is

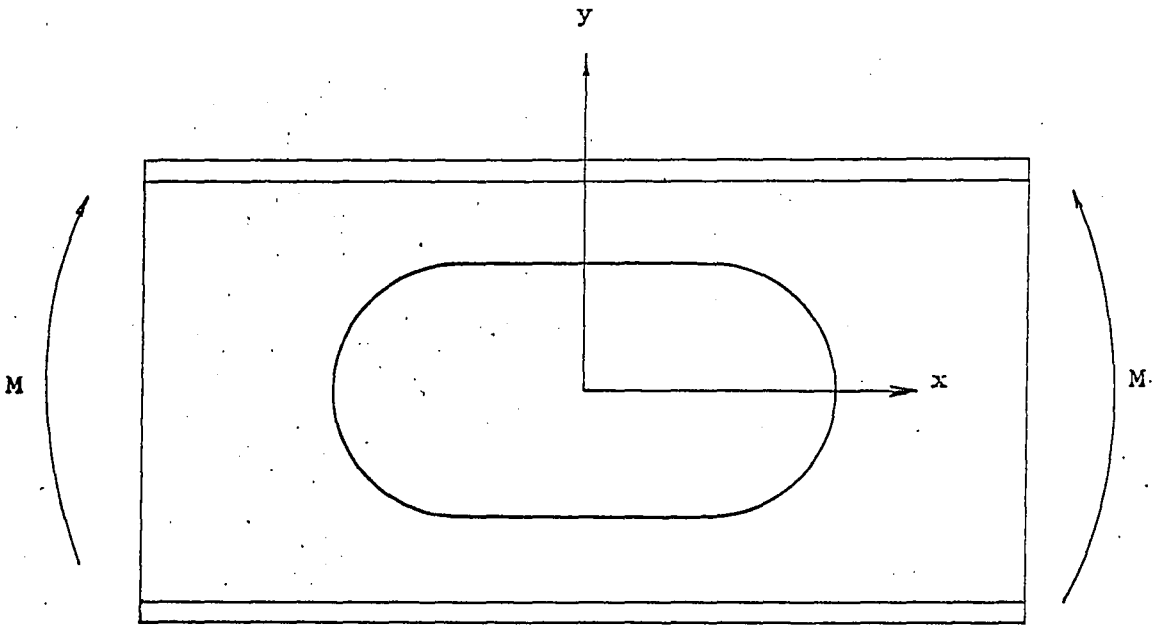

(a) Beam Element Near the Opening Subjected to Pure Bending.

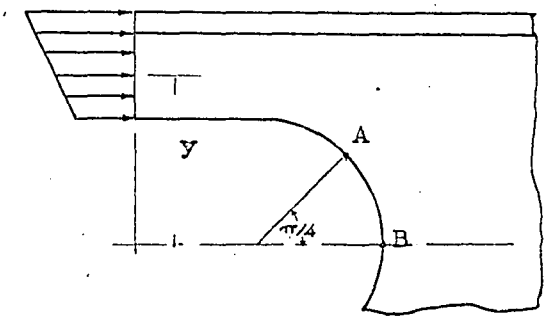

(b) Quarter Free Body.

Fig. 2-2

the moment at the centre of the opening, and I_n is the moment of inertia of the net section of the wide-flange beam at the centre of the opening. Besides, the shear stresses vanish at the central section of the ring since the structure and loadings are symmetrical about the y-axis. Then, by considering the free body shown in Figure 2-2b, the stresses at the boundary of the opening can be found by conventional methods. The tangential stress at the curved boundary can be obtained by first finding the axial stress on the vertical section, still based on the assumption of plane sections remaining plane, and then resolving it into the tangential direction. However, this approximate method is only valid approximately up to the quarter point (point A as shown in Figure 2-2b) of the half-circular boundary, for the slope of the tangent becomes steeper and steeper which makes the stress at point B infinity, and certainly this contradicts the actual situation.

2.2 PURE SHEAR

1. Small Hole Theory

Heller et al. have also derived a formula[23] which is shown below for calculating the stresses for the case of pure shear

$$J_o^2 \sigma_t = \frac{RA^2}{2I} (\Delta_2 \sin 2\beta + \Delta_4 \sin 4\beta + \Delta_6 \sin 6\beta + \Delta_8 \sin 8\beta + \Delta_{10} \sin 10\beta) \qquad (2\text{-}3)$$

where R is the shear force (Figure 2-3a) and

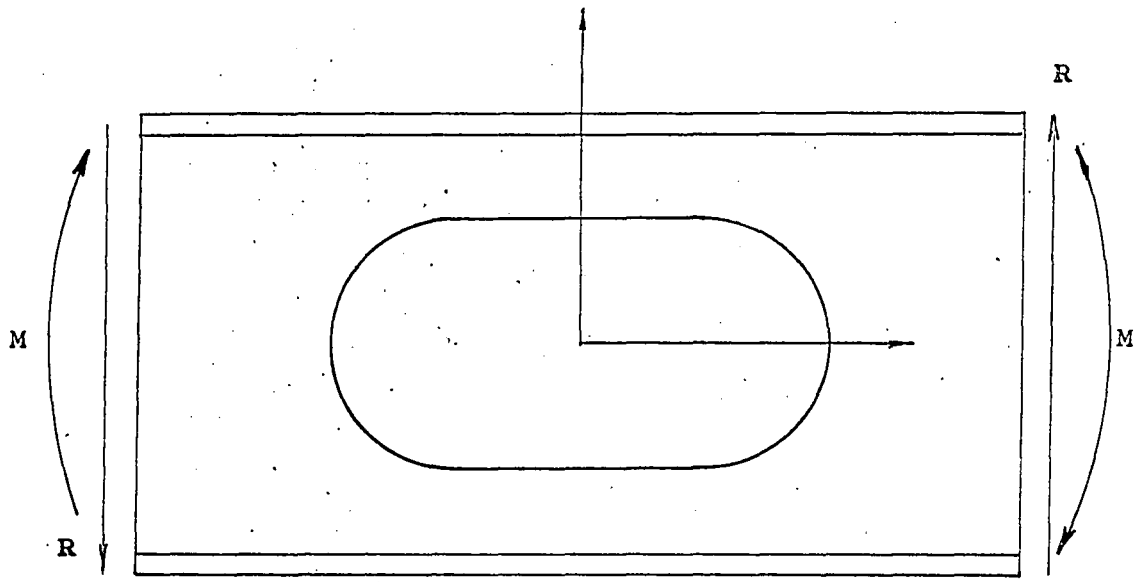

(a) Beam Element Near the Opening Subjected to Pure Shear.

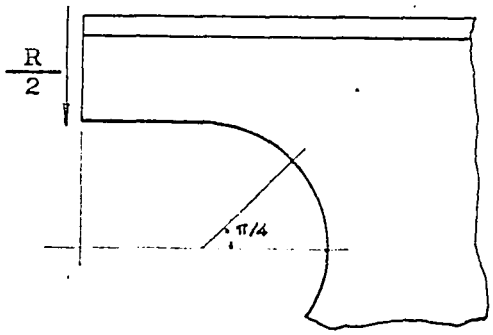

(b) Quarter Free Body.

Fig. 2-3

$$\Delta_2 = A^2 + a_1'' A^2 - 3a_3'' AB + 3a_1'' AC - 15a_5'' AC + 15a_3'' AD - 35 K_3 AD + 35a_5'' AE - 63E^2$$

$$\Delta_4 = 3a_3'' A^2 - AB - 5a_5'' AB - 21 K_3 AC + 5a_1'' AD - 45DE + 21a_3'' AE$$

$$\Delta_6 = 5a_5'' A^2 - 7 K_3 AB - 3AC - 27CE + 7a_1'' AE$$

$$\Delta_8 = 2(AD - BE)$$

$$\Delta_{10} = 2AE$$

$$a_1'' = \frac{\frac{K_3(2 - 3 K_7)}{1 + 3K_1} + K_9 - 5 K_1 K_5 - \frac{8I\tau\Gamma}{RA^2}}{1 + K_5 - \frac{3 K_3^2}{1 + 3 K_1} - 5 K_1^2}$$

$$a_3'' = - \frac{1}{1 + 3 K_1} \left(K_3 a_1'' + \frac{2 - 3 K_7}{3} \right)$$

$$a_5'' = K_5 - K_1 a_1''$$

$$K_9 = 1 + \frac{B}{A} K_7 + \frac{3C}{A} K_5 + \frac{5D}{A} K_3 + \frac{7E}{A} K_1$$

$$\tau = \frac{R}{A_w}$$

$$\Gamma = \frac{3}{2\left(1 - \frac{t_f}{h}\right)} - \frac{A_w h^2}{2I} \cdot \frac{A_f/A_t}{1 - A_f/A_t}$$

A_w = gross area of web

A_f = gross area of flange

A_t = total area of beam

h = half height of beam.

2. Ring Theory

In contrast to the case of pure bending, the structural element shown in Figure 2-3a subjected to antisymmetric loadings (pure shear) is actually a statically determinant structure. Then, one can readily conclude from its symmetry that both the axial and moment forces acting at the centroid of the tee vanish at the central section on which the shear force is equal to R/2. Hence, by a similar procedure as in the case of pure bending, the stresses at the boundary can be obtained by examining the free body shown in Figure 2-3b. However, when the web depth is small compared with the flange width, the effective width of the flange must be taken into consideration since a non-uniform stress distribution will exist across the width of the flange[32].

2.3 BENDING WITH SHEAR

As shown in Figure 2-4, the stresses for the case of bending with shear can be obtained by superposition of pure bending and pure shear, either by small hole theory or by ring theory, or by a combination of these.

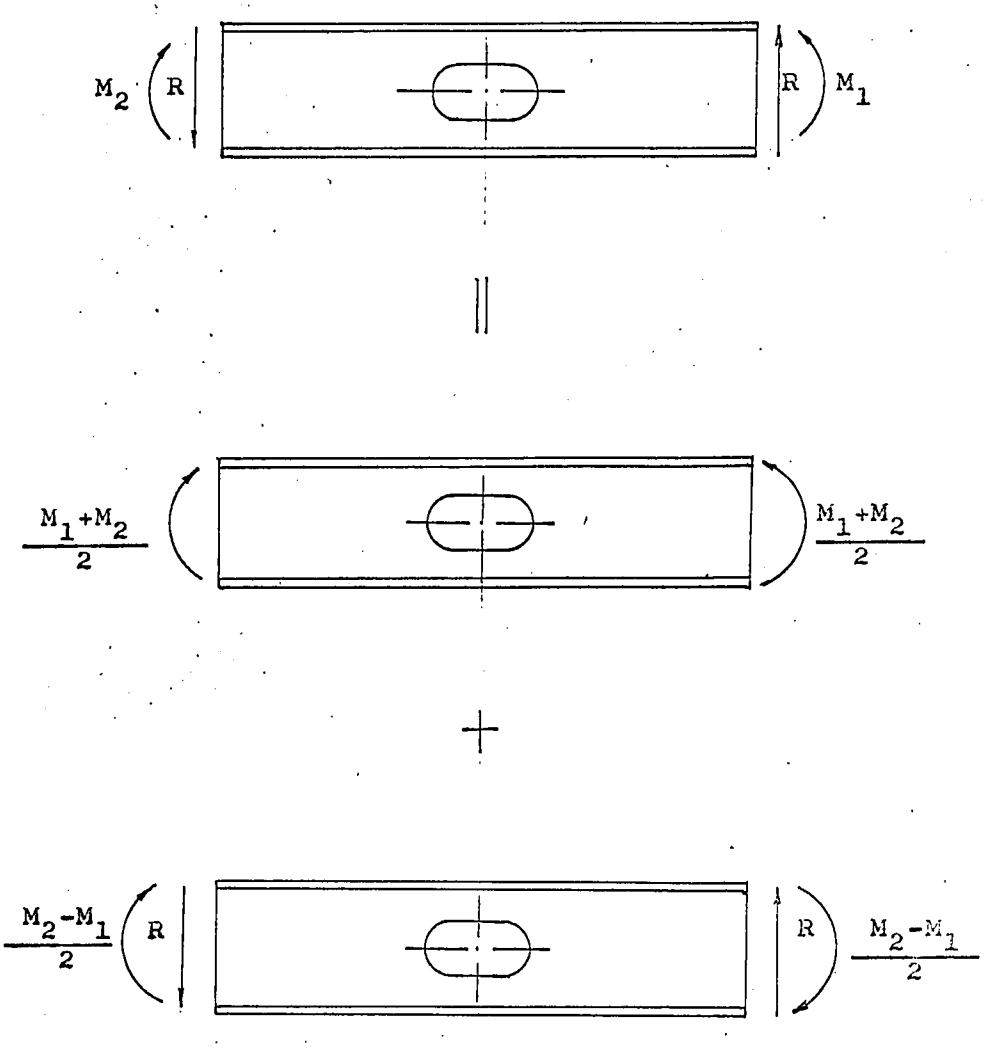

Fig. 2-4 Superposition Diagram.

CHAPTER III

THEORETICAL APPROACHES - ULTIMATE STRENGTH

The ultimate strength of a wide-flange beam with an extended opening is analyzed both for pure bending and bending with shear. The material of the beam is assumed to be ideally plastic, i.e. no strain hardening occurs throughout stress-strain range up to failure. For the case of pure bending, it is assumed that one plastic hinge is formed at the centre of the opening, while for bending with shear either one or four plastic hinges are assumed to be formed at the opening, depending on the shear moment ratio at the opening as well as the dimensions of the hole and the beam section. In addition, shear, axial and moment forces are all taken into consideration at the yield sections in order to keep every free body taken from the beam in equilibrium.

3.1 PURE BENDING

The plastic behaviour of a wide-flange beam with an extended opening subjected to pure bending is investigated as follows: As shown in Figure 3-1, the whole section of the shaded portion above and below the opening reaches the yield stress. Thus, by the equilibrium condition, the ultimate load P can be directly found as follows:

$$P = \frac{2A_t h_c \sigma_{y.p.}}{L} \qquad (3\text{-}1)$$

where A_t is the area of the smallest tee section above and below the

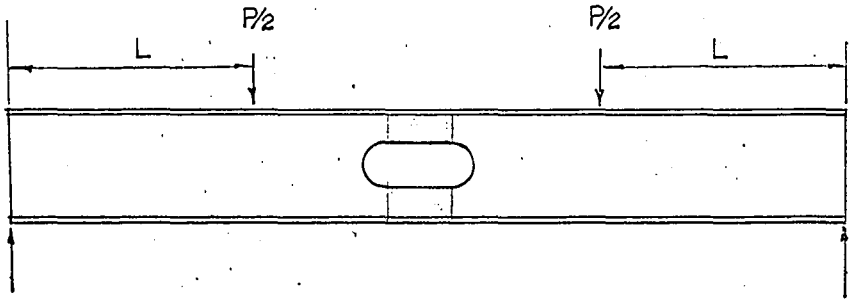

Fig. 3-1 Possible Type of Failure for Pure Bending.

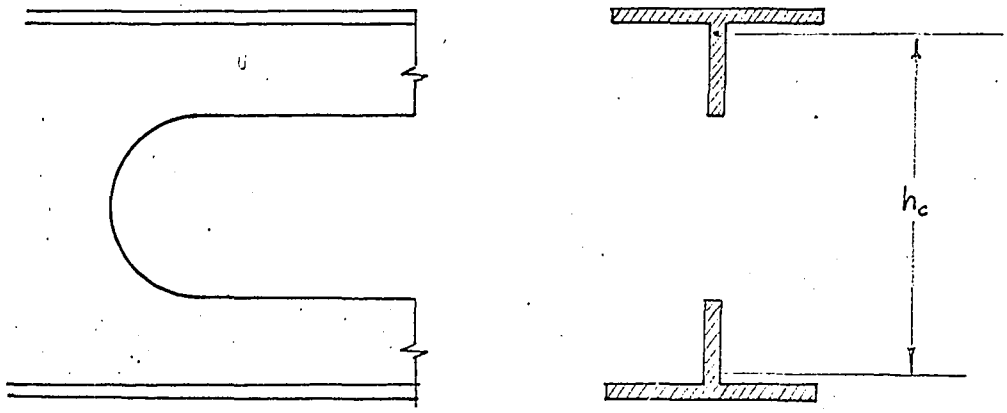

Fig. 3-2 Beam Section through the Opening.

opening, $\sigma_{y.p.}$ is the yield point stress in tension, and h_c is the distance between the centroids of upper and lower tee sections (Figure 3.2).

3.2 BENDING WITH SHEAR

1. Possible Types of Failure

Depending on the ratio of shear to moment at the opening as well as the dimensions of the opening and the beam section, four possible types of failure are hypothesized for the case of bending with shear. The beam may fail

i. by a four plastic hinge mechanism as shown in Figure 3-3a when the ratio of shear to moment at the opening is high;

ii. by local inelastic buckling at A and B as shown in Figure 3-3a when the shear moment ratio is high;

iii. by a one plastic hinge mechanism as shown in Figure 3-3b when the shear moment ratio is low, and

iv. by a one plastic hinge mechanism as shown in Figure 3-3c when the shear moment ratio is low and the dimension of the opening is small compared with the depth of beam.

The ultimate load for Type iv failure can be calculated by the conventional method, but the behaviour of Type ii failure is rather complicated and is beyond the scope of this thesis. Hence, only Type i and Type iii are investigated in the following sections.

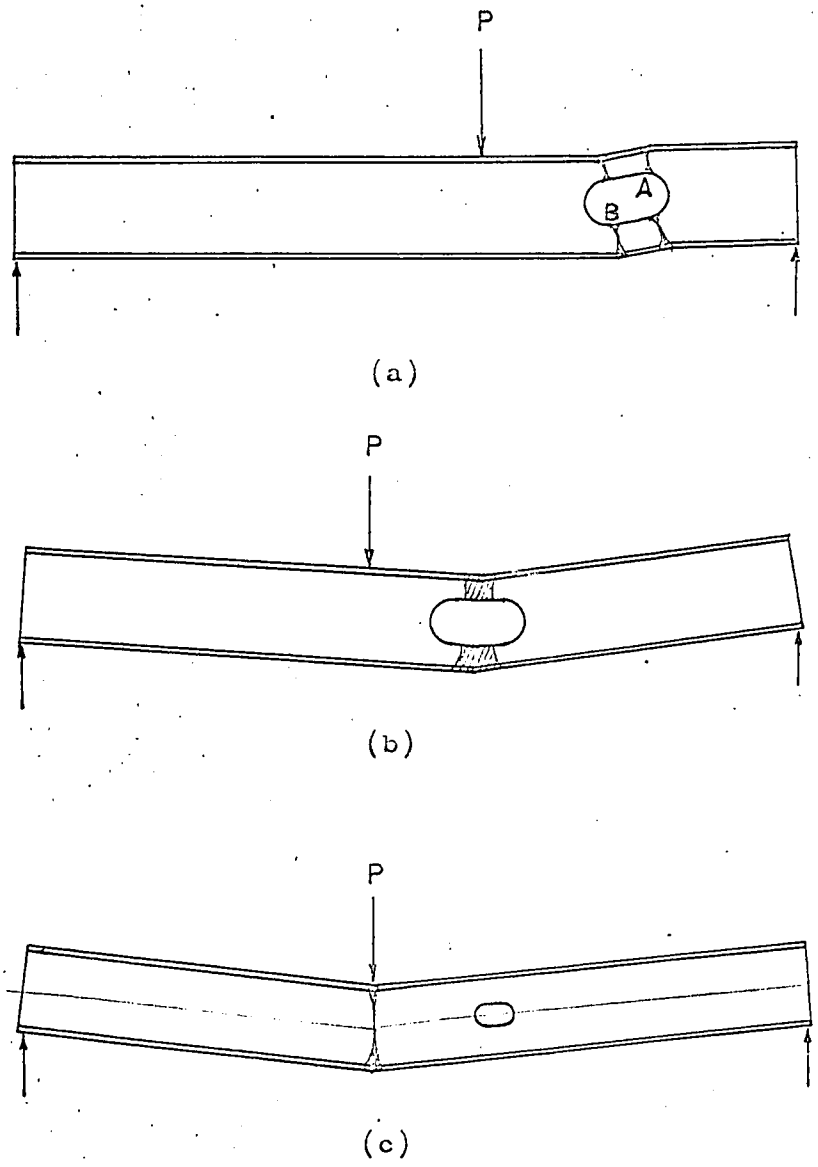

Fig. 3-3 Possible Types of Failure for Bending with Shear

2. Four Hinge Mechanism - High Shear Moment Ratio

Since the shear moment ratio is high, the bending stress at the yield sections due to the shear force is larger than the stress due to axial force. Hence the stress distribution at these sections should be partly in tension and partly in compression. In order to make the problem simplified and solvable, the following assumptions were made, some of which are fully discussed at the end of this chapter. These assumptions are:

a. The four plastic hinges are located at the tangent points as shown in Figure 3-4.

b. The stresses on the yield sections are distributed in the way shown in Figure 3-5a, i.e. part of the section yields in direct stress, and part of it by shear.

c. The shear yield stress is determined from the distortion energy yield criterion, i.e.

$$\sigma_x^2 + 3\tau_{xy}^2 = \sigma_{y.p.}^2 \qquad (3\text{-}2)$$

where σ_x is the axial stress, and τ_{xy} the shear stress. Thus, for pure shear,

$$\tau_{y.p.} = \frac{\sigma_{y.p.}}{\sqrt{3}} \qquad (3\text{-}3)$$

in which $\tau_{y.p.}$ is shear yield stress.

d. The plastic moments about the axis through the centroid of tee section at the four hinges are equal. Thus the points of inflection fall at the mid-length of the opening.

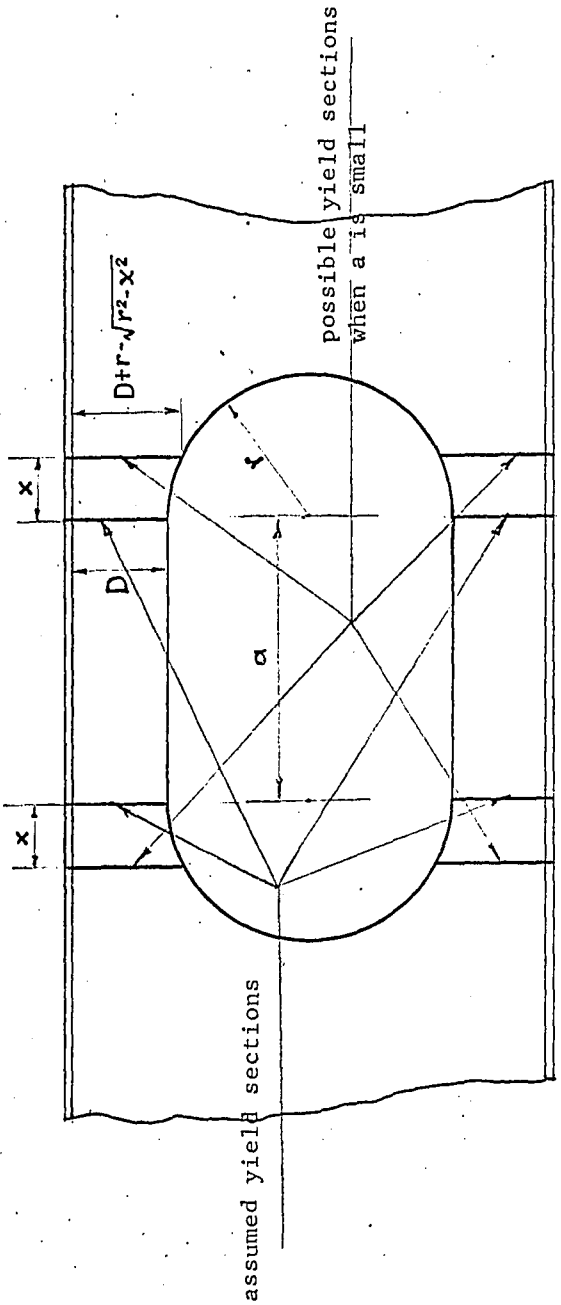

Fig. 3-4 Possible Locations of the Yield Section.

e. The opening is far away from the applied load and the reaction, so that the effect of the stress concentrations due to the concentrated loading can be neglected. Thus, by the symmetric property of the geometrical configuration, the total shear force at the opening should be equally carried by the upper and lower tee sections.

Figure 3-5a is a free body diagram bounded by two yield sections as shown in Figure 3-4. From assumption (c) we get

$$k_3 = D - \frac{\sqrt{3}\ R}{2t_w \sigma_{y.p.}} \tag{3-4}$$

in which D is the web depth of the tee section, t_w is the web thickness, and R is the right reaction of the beam (Figure 3-5b). In addition, by equilibrium of all the horizontal forces, one obtains

$$\sigma_{y.p.}[bk_1 - b(t_f - k_1) - k_3 t_w] = \sigma_{y.p.}[t_w k_3 + b\, t_f - k_2) - bk_2] \tag{3-5}$$

in which t_f is the flange thickness of the tee section. Substituting (3-4) in (3-5) and rearranging, equation (3-5) becomes

$$k_1 + k_2 = t_f + \frac{Dt_w}{b} - \frac{\sqrt{3}\ R}{2b\,\sigma_{y.p.}} \tag{3-6}$$

Moreover, by equilibrium of all moment forces about the horizontal axis through the centroid of tee section, we get

$$b\,\sigma_{y.p.}\left[2(D - \bar{y} + t_f)\left(t_f + \frac{Dt_w}{b} - \frac{\sqrt{3}\ R}{2b\,\sigma_{y.p.}}\right) - 2t_f\left(D - \bar{y} + \frac{t_f}{2}\right)\right.$$
$$\left. - k_1^2 - k_2^2\right] + 2t_w \sigma_{y.p.}\left(D - \frac{\sqrt{3}\ R}{2t_w \sigma_{y.p.}}\right)\left[\bar{y} - \frac{1}{2}\left(D - \frac{\sqrt{3}\ R}{2t_w \sigma_{y.p.}}\right)\right]$$
$$= \frac{Ra}{2} \tag{3-7}$$

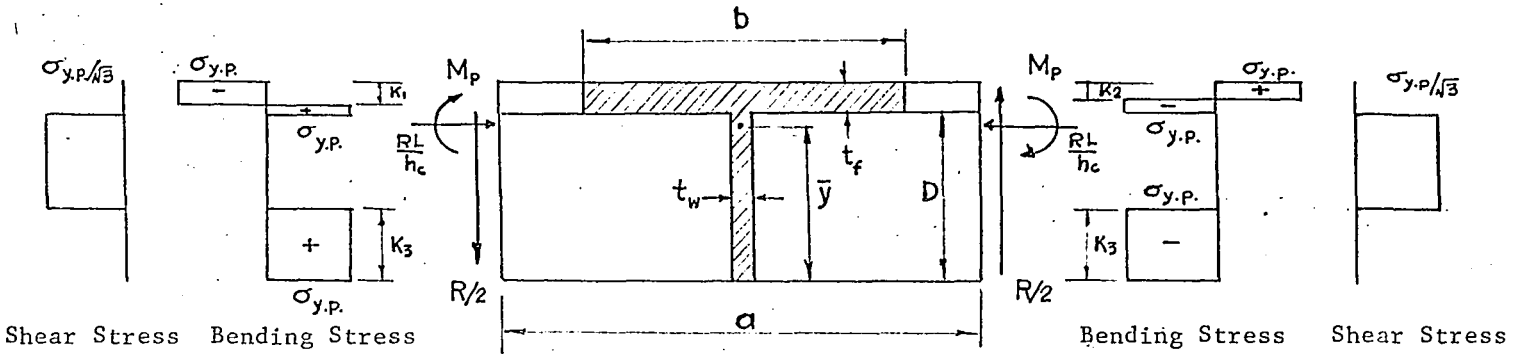

(a) The Free Body Bounded by Two Yield Section.

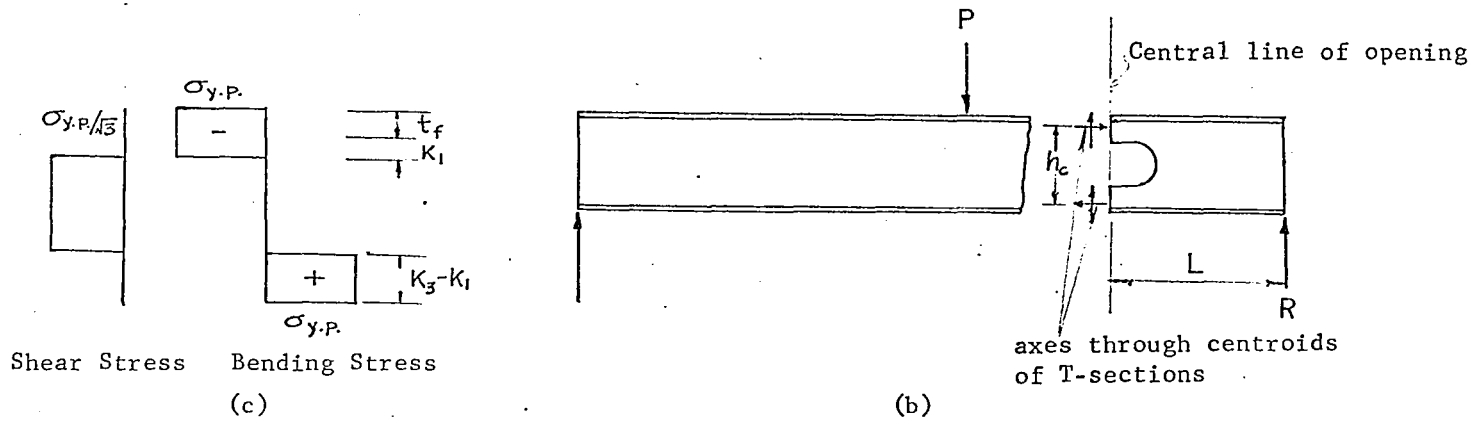

Fig. 3-5 Beam Failure by a Four Hinge Mechanism.

in which $\bar{y}$ is the distance from the boundary of the opening to the centroid of the tee. One more equation can be obtained by considering the equilibrium of the right-hand side free body shown in Figure 3-5b, i.e.

$$b\,\sigma_{y.p.}(2k_1 - t_f) - \left(D - \frac{\sqrt{3}\,R}{2t_w\,\sigma_{y.p.}}\right)t_w\,\sigma_{y.p.} = \frac{RL}{h_c} \qquad (3\text{-}8)$$

in which h_c is the distance between the centroids of upper and lower tees. Eliminating k_1 and k_2 from equations (3-5), (3-6) and (3-8), the following quadratic equation is obtained for R

$$\left(\frac{3}{4} + \frac{L^2}{h_c^2} + \frac{3b}{2t_w}\right)R^2 + \sigma_{y.p.}(ab + \sqrt{3}\,bt_f - \sqrt{3}\,Dt_w)R$$

$$+ \sigma_{y.p.}^2\,[D^2t_w^2 - b^2t_f^2 - 2bDt_w(D + t_f)] = 0 \qquad (3\text{-}9)$$

The solution of equation (3-9) is the value of R corresponding to the ultimate strength of the beam. Since the equation is quadratic, two solutions exist. However, one of them is negative and meaningless.

Substituting R in equations (3-6) and (3-8), we can get the values of k_1 and k_2. However, it should be noticed that equation (3-9) only holds true when $0 < k_1 \leqslant t_f$ and $0 < k_2 \leqslant t_f$. For $k_1 > t_f$, the stresses on the left yield section (Figure 3-5a) should be distributed in the way shown in Figure 3-5c. Following a similar procedure as indicated before, we obtain another quadratic equation as follows:

$$\left[\left(\frac{L}{h_c}+\frac{\sqrt{3}}{2}\right)\left(\frac{\sqrt{3}}{2b}+\frac{L}{bh_c}+\frac{L}{ht_w}\right)-\left(\frac{L}{h_c}-\frac{\sqrt{3}}{2}\right)\frac{\sqrt{3}}{2t_w}\right]R^2$$

$$+\left[\sqrt{3}\left(\frac{t_f}{2}+8D-8\bar{y}-\frac{Dt_w}{b}\right)+\frac{L}{h_c}\left(t_f+2D-\frac{2Dt_w}{b}-\frac{2bt_f}{t_w}\right)+2a\right]\sigma_{y.p.}R$$

$$-\left[t_f b\left(D+3t_f-\frac{Dt_w}{b}-\frac{bt_f}{t_w}\right)+Dt_w\left(9D-8\bar{y}+3t_f-\frac{Dt_w}{b}+\frac{t_f b}{t_w}\right)\right]\sigma_{y.p.}^2$$

$$=0 \qquad (3\text{-}10)$$

One of the two solutions of equation (3-10) is the correct value of R, provided that its corresponding values of k_1 and k_2 satisfy the conditions that $0 < k_1 \leq D$ and $0 < k_2 \leq t_f$.

3. <u>One Hinge Mechanism - Low Shear Moment Ratio</u>

When the shear moment ratio is low, the whole tee may be in compression or tension. By considering the effect of shear force and keeping all forces acting on the free body element in equilibrium, we assume a simplified stress distribution which is shown in Figure 3-6a, while the assumption concerning shear force distribution and shear yield stress are the same as before. From the equilibrium of the right hand side free body shown in Figure 3-6b, we get

$$R\left(L-\frac{a}{2}\right)=2\sigma_{y.p.}\left[bt_f\left(\frac{H}{2}-\frac{t_f}{2}\right)+Dt_w\left(\frac{H}{2}-t_f-\frac{D}{2}\right)\right.$$

$$\left.-\frac{\sqrt{3}R}{2t_w\sigma_{y.p.}}t_w\left(\frac{H}{2}-t_f-\frac{\sqrt{3}R}{4t_w\sigma_{y.p.}}\right)\right] \qquad (3\text{-}11a)$$

where H is the total depth of the beam. Rearranging equation (3-11a) yields

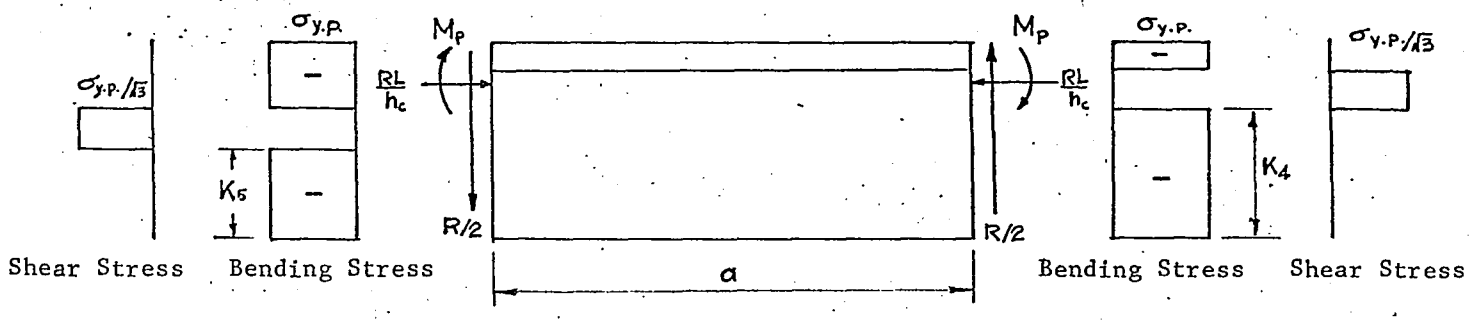

(a)

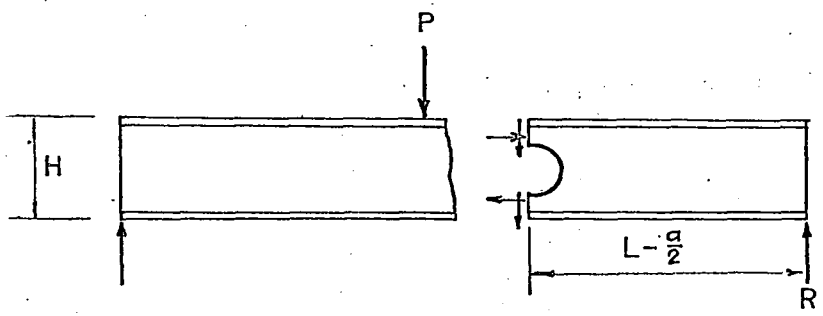

(b)

Fig. 3-6 Beam Failure by a One Hinge Mechanism.

$$\frac{3}{4t_w \sigma_{y.p.}} R^2 - \left[\frac{\sqrt{3}}{2}(H - 2t_f) + L - \frac{a}{2}\right]R + bt_f \sigma_{y.p.}(H - t_f)$$

$$+ Dt_w \sigma_{y.p.}(H - 2t_f - D) = 0 \qquad (3\text{-}11)$$

The solution of equation (3-11) is the value of R corresponding to the ultimate strength of the beam. Depending on the size of the opening as well as the ratio of shear to moment, either one or none of the two solutions is correct. From consideration of the equilibrium of the free body shown in Figure 3-6a, the following is obtained.

$$k_5 = D - \frac{\sqrt{3}\,R}{2t_w \sigma_{y.p.}} - \frac{a}{\sqrt{3}} \qquad (3\text{-}12)$$

Hence, the correct value of R should be the one which makes k_5, by substituting R in equation (3-12), greater than or equal to zero.

4. Criterion for Different Types of Failure

Putting k_5 equal to zero in equation (3-12) yields

$$D - \frac{a}{\sqrt{3}} = \frac{\sqrt{3}\,R}{2t_w \sigma_{y.p.}} \qquad (3\text{-}13)$$

From equations (3-11) and (3-13), we get the critical value of L, say L_c, as follows:

$$L_c = \frac{3[bt_f(H - t_f) + Dt_w(H - 2t_f - D)]}{2t_w(\sqrt{3}\,D - a)} - \frac{\sqrt{3}}{2}(H - 2t_f - D) \qquad (3\text{-}14)$$

Since k_5 shown in Figure 3-6a should always be positive, it follows from equation (3-12) that

$$D > \frac{a}{\sqrt{3}} \tag{3-15}$$

and

$$\frac{\sqrt{3}\,R}{2t_w \sigma_{y.p.}} < D - \frac{a}{\sqrt{3}} \tag{3-16}$$

Therefore, with all the assumptions made in the foregoing sections, an approximate criterion for different types of failure can be obtained as follows: when $D > \frac{a}{\sqrt{3}}$ and $L > L_c$, the beam will fail by the one hinge mechanism; and when $D \leqslant \frac{a}{\sqrt{3}}$ or when $D > \frac{a}{\sqrt{3}}$ and $L \leqslant L_c$, the beam will fail by the four hinge mechanism.

5. Discussion

The foregoing methods for calculating ultimate loads for different types of failure are rather ideal analyses, i.e. all have been based on the common assumption that the material of the wide-flange beam is ideally plastic. Actually, the pattern of stress distribution shown in Figures 3-5 and 3-6a cannot be attained, for excess strain near the boundary of opening would cause strain hardening in this region. Moreover, it is possible that the beam may fail by local inelastic buckling in the web, with its strain somewhere in the strain hardening range, while the flange is still below the yield point stress. However, with the ideal plastic material assumed, the patterns of stress distribution seem to be the most reasonable which permit a straightforward solution to be obtained. Except at points of discontinuous stress, the two equilibrium equations for plane stress are both satisfied throughout the section. The two equations are

$$\frac{\partial \sigma_x}{\partial x} + \frac{\partial \tau_{xy}}{\partial y} = 0$$

$$\frac{\partial \sigma_y}{\partial y} + \frac{\partial \tau_{xy}}{\partial x} = 0 \qquad (3\text{-}17)$$

where σ_x and σ_y are the direct and normal stresses and τ_{xy} is the shear stress. Again, elastic analysis indicates that high strain concentrations occur on the boundary of the opening, so it is logical to conclude that the portion of the web near the boundary will yield by bending stress. Finally, experiments by Bower[30] have shown that the upper part of the web above an opening does yield in pure shear. Hence, and since the effect of strain hardening is neglected, the foregoing analyses for different types of failure are approximately lower bounds and thus conservative solutions.

The yield point stress of the material of the wide-flange beam actually varies from point to point. Some experiments[30] showed that the yield point stress of the flange was much lower than that of the web. If different values of yield point stress for the flange and the web are used, then equation (3-9) becomes

$$\left[\frac{3}{4} + \frac{L^2}{h_c^2} + \frac{3bY_f}{2t_wY_w}\right]R^2 + [abY_f + 3\,bt_fY_f - 3\,Dt_wY_w]R$$
$$+ [D^2t_w^2Y_w^2 - b^2t_f^2Y_f - 2bDt_w(D + t_f)Y_fY_w] = 0 \qquad (3\text{-}9a)$$

in which Y_f is the yield point stress of the flange and Y_w that of the web. Results of numerical calculations based on an arbitrarily assumed

ratio of Y_f to Y_w are shown in Chapter V.

When 'a' is small, the yield sections may be shifted to the positions shown in Figure 3-4, then equation (3-9) should be modified and written as

$$\left[\frac{3}{4} + \frac{L^2}{h_c^2} + \frac{3b^2}{2t_w}\right]R^2 + \sigma_{y.p.}\left[(a + 2x)b + \sqrt{3}bt_f - \sqrt{3}t_w(D + r - \sqrt{r^2 - x^2})\right]R$$

$$+ \sigma_{y.p.}^2\left[(D + r - \sqrt{r^2 - x^2})^2 t_w^2 + b^2 t_f^2\right.$$

$$\left. - 2bt_w(D + r - \sqrt{r^2 - x^2})(D + t_f + r - \sqrt{r^2 - x^2})\right] = 0 \qquad (3\text{-}9b)$$

in which x is a variable indicating the distance between the assumed and shifted positions. Solving R from equation (3-9b) as a function of x, and minimizing R with respect to x, we can get the x and corresponding R which is the correct solution of equation (3-9b). If we put 'a' equal to zero in equation (3-9b), then a quadratic equation for the case of a circular opening can be obtained as follows:

$$\left[\frac{3}{4} + \frac{L^2}{h_c^2} + \frac{2b}{2t_w}\right]R^2 + \sigma_{y.p.}\left[2bx + \sqrt{3}bt_f - \sqrt{3}t_w(D + r - \sqrt{r^2 - x^2})\right]R$$

$$+ \sigma_{y.p.}^2\left[(D + r - \sqrt{r^2 - x^2})^2 t_w^2 + b^2 t_f^2\right.$$

$$\left. - 2bt_w(D + r - \sqrt{r^2 - x^2})(D + t_f + r - \sqrt{r^2 - x^2})\right]$$

$$= 0 \qquad (3\text{-}18)$$

The correct values of x and R can again be calculated by minimizing R

with respect to x.

Equations (3-9), (3-10) and (3-11) can also be applied to the beam with rectangular opening, with 'a' being the horizontal length of the hole. In addition, by putting 'a' equal to zero, equation (3-11) becomes

$$\frac{3}{4t_w \sigma_{y.p.}} R^2 - \left[\frac{\sqrt{3}}{2}(H - 2t_f) + L\right]R + bt_f \sigma_{y.p.}(H - t_f)$$

$$+ Dt_w \sigma_{y.p.}(H - 2t_f - D) = 0 \qquad (3\text{-}19)$$

This is for the case of the circular opening if the beam fails by a one plastic hinge mechanism.

CHAPTER IV

EXPERIMENTAL PROCEDURE

4.1 GENERAL DESCRIPTION

Two specimens of A 36 steel 14"WF at 30 lb beams each with a single extended opening as shown in Figure 4-1 were tested to investigate their elastic and plastic behaviour under different loading conditions. Specimen A, 15 feet long, was subjected to pure bending (Test No. 1), shown in Figure 4-2, while specimen B which was 19 feet long was tested under different ratios of shear to moment (Tests Nos. 2 to 4, as shown in Figure 4-2).

Measurements of deflections and elastic strains under different loading conditions and at various stages of loading were recorded and also the ultimate strength of the beams.

Both electrical resistance strain gauges and a photo-elastic coating (Photostress) were employed to measure the elastic strains in the web around the opening. The loading was applied by a 440 kips capacity Baldwin-Emery testing machine in the form of one or two (pure bending) concentrations on a 14 foot span. Load was increased at the rate of 5 kips per minute.

4.2 MEASUREMENT OF ELASTIC STRAIN

1. Strain Gauge Method

Two kinds of foil strain gauges produced by Budd

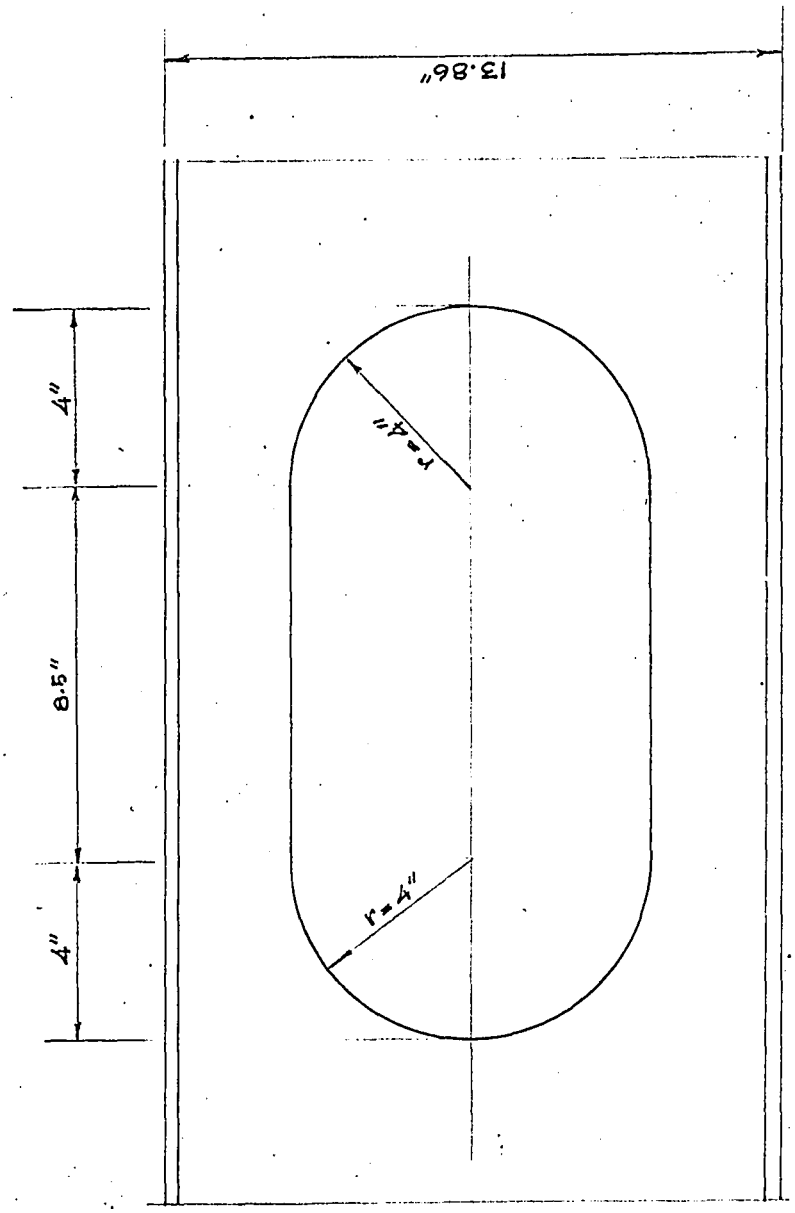

Fig. 4-1 Dimensions of the Opening.

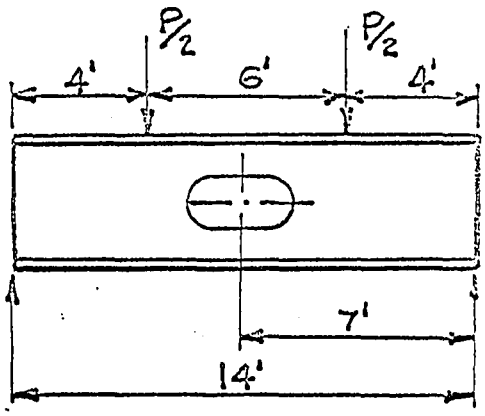

TEST NO. 1

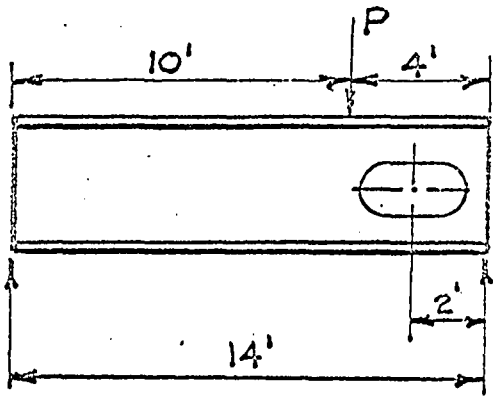

TEST NO. 2

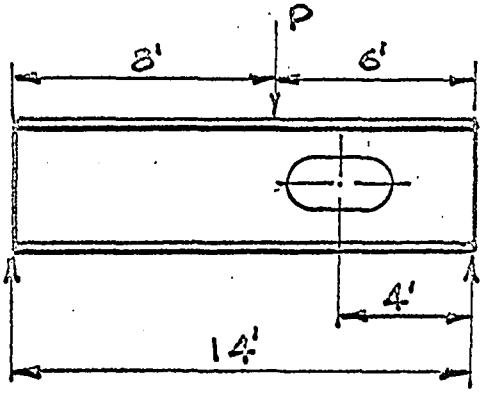

TEST NO. 3

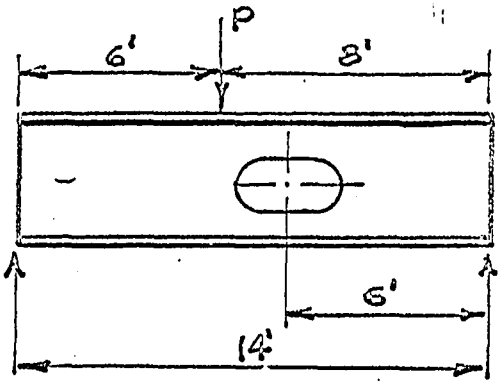

TEST NO. 4

FIGURE 4-2

TEST LAYOUT

Instruments Limited were used to measure the elastic strains of the tested specimens. The linear gauges C6-121A were mounted on the boundaries of openings, while C6-121-R3C, which are 120^{o} rosette gauges, were bonded to the interior points around the holes. Linear and rosette gauges were also mounted on the flange surface of specimens A and B respectively. The detailed locations of all the gauges both on specimens A and B are shown in Figures 4-3 and 4-4.

Strains were recorded with Model A-110 digital strain indicator (Budd Instruments Ltd), by using a half bridge circuit with a dummy gauge mounted on the plate which was cut from the opening in the web.

Measurement of relative strain has been adopted throughout the experiments, i.e. the strains indicated for some particular loading are actually the additional strains due to the additional loadings. In the case of pure bending, zero strain readings were set when an initial loading of 2 kips had been applied. Further records were taken at increments of 10 kips until a final load of 42 kips was obtained. For the case of bending with shear, 1 kip was taken as the initial loading, and further records were taken at increments of 5 kips until a final load of 11 kips (Tests Nos. 2 and 3) or 16 kips (Test No. 4) was applied.

Since all the gauges were placed only on one side of the neutral axis of the beam, the strains measured were limited to this side.

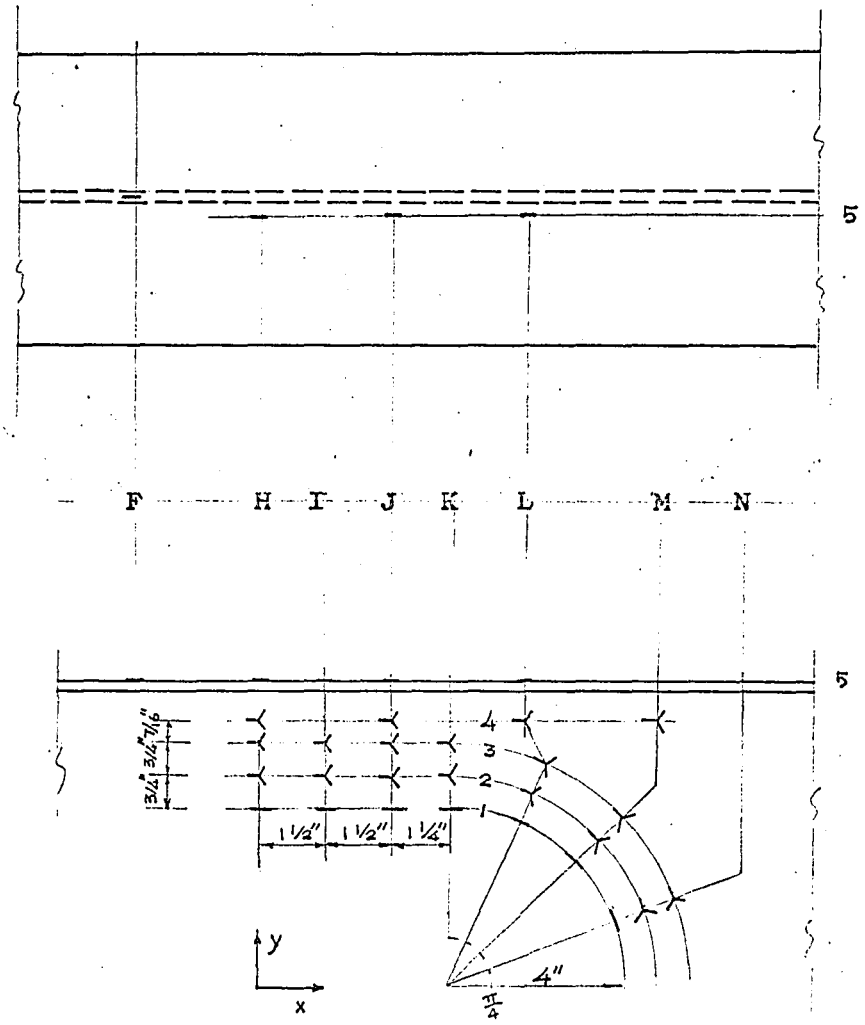

Fig. 4-3 Locations of the Strain Gage on Specimen A.

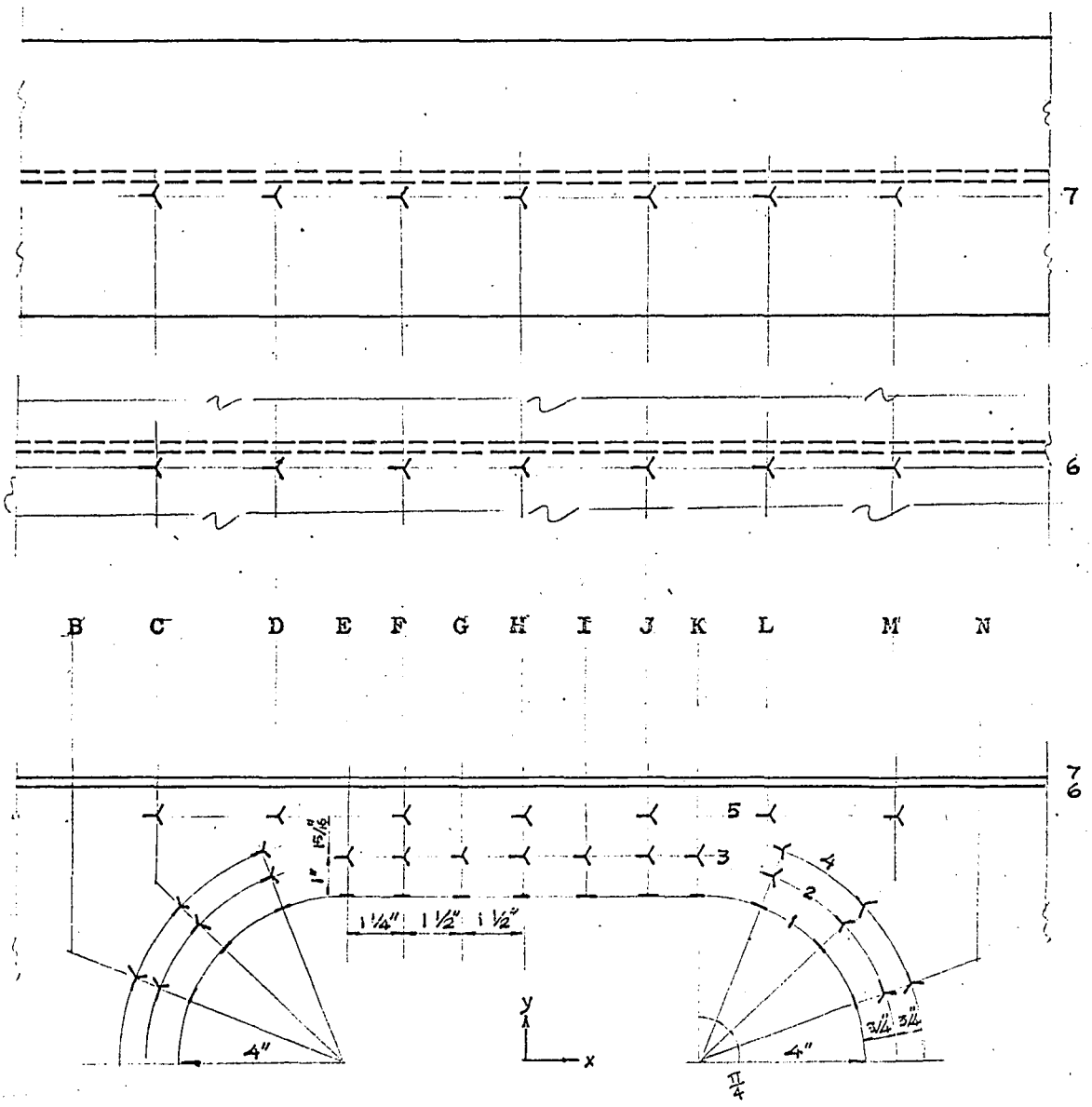

Fig. 4-4 Locations of the Strain Gage on Specimen B.

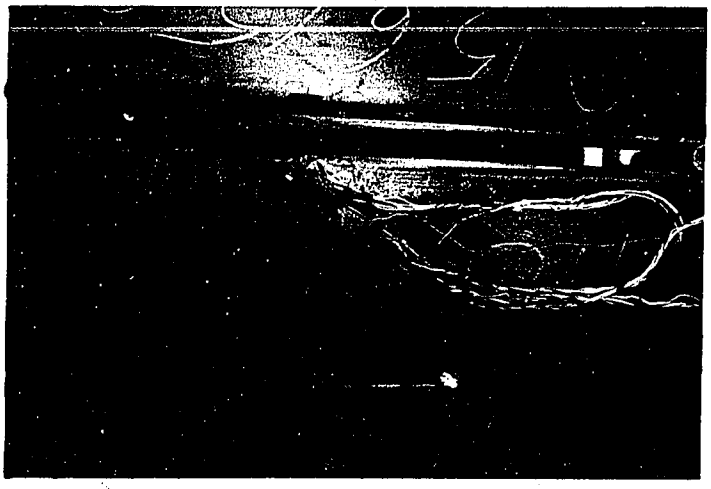

PLATE 4-1

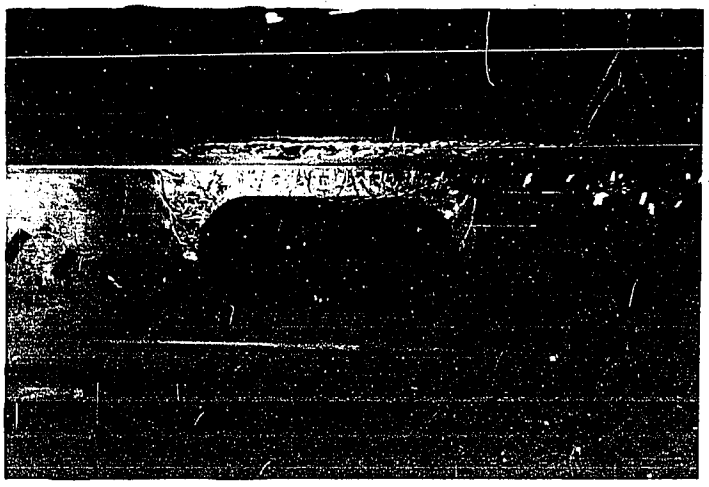

PLATE 4-2

PLATE 4-1

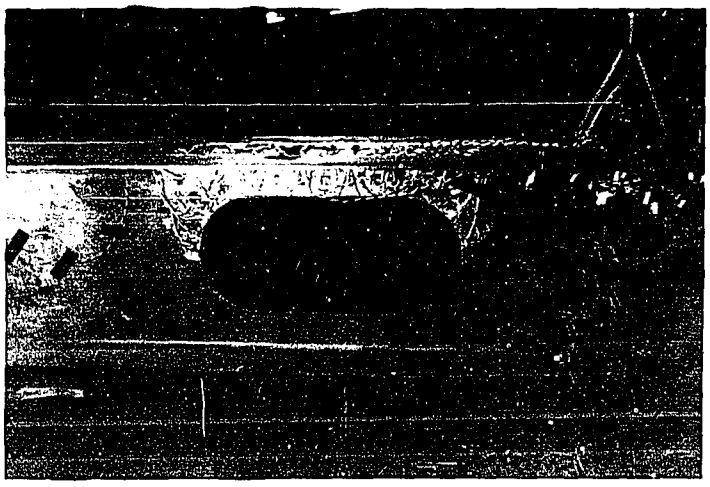

PLATE 4-2

However, strains on the other side of the axis were also obtained by turning the beam upside down and repeating the procedure mentioned before.

2. Photostress Method

In addition to strain gauge measurements, the tangential strains on the boundary of the opening were also measured by the photostress method. The photostress technique is more economical than the strain gauge method in view of money and time. Actually it contains infinite numbers of gauges over the region of particular interest. Both in specimens A and B type S plastic sheets (K factor = 0.093, thickness = 0.120") cut in the shapes shown in Figure 4-5 were bonded to the web surface around the openings, using reflecting cement. Before bonding the cut plastic sheets were checked by polarizer and analyzer and there was no residual fringe induced by improper cutting. Fringe orders at particular points on the boundary of the opening were measured with a large field meter (Budd Instruments Ltd.). According to the theory of photoelasticity[31], the tangential unit strain at a free boundary can be obtained as follows:

$$e_t = \frac{1}{1+\mu_s} \frac{\nearrow N_n}{2t_p K F_c} \qquad (4\text{-}1)$$

where e_t = tangential unit strain at free boundary

μ_s = Poisson's ratio of sample beam

N_n = fringe order in normal incidence which can be measured with the large field meter

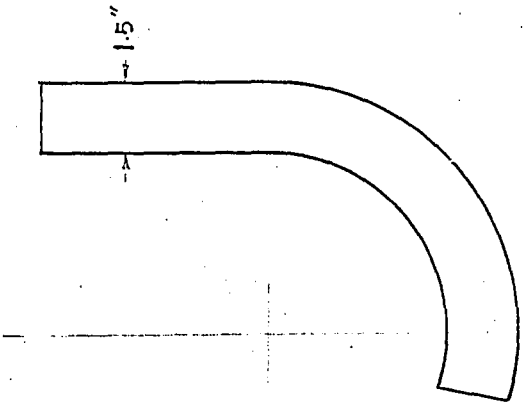

(a) Specimen A

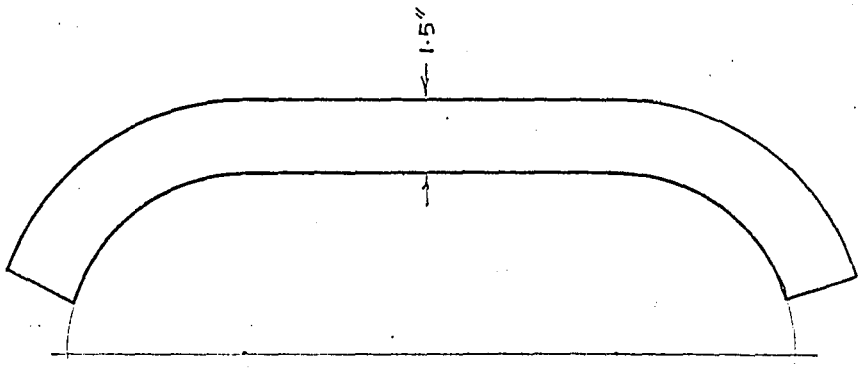

(b) Specimen B

Fig. 4-5 The Cut Plastic Sheets.

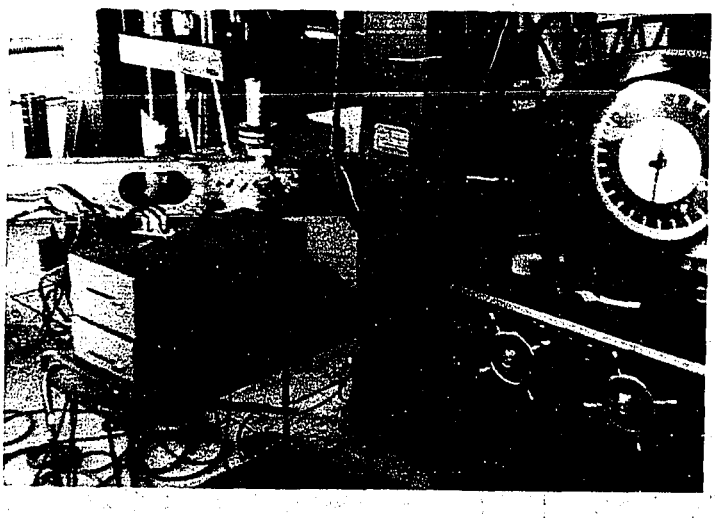

PLATE 4-3

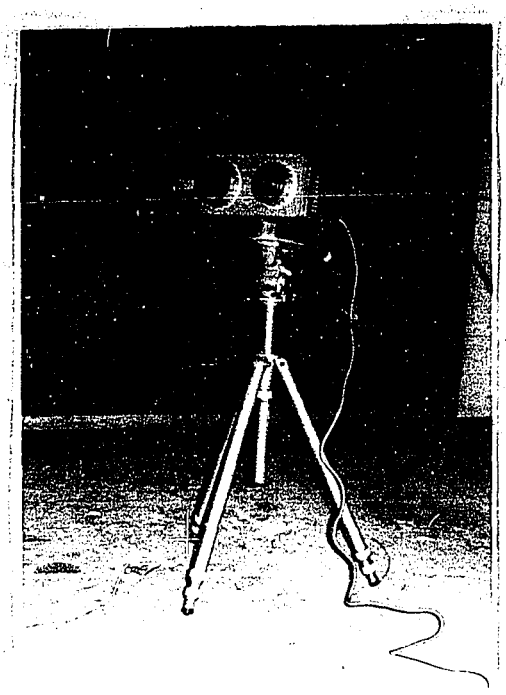

PLATE 4-4

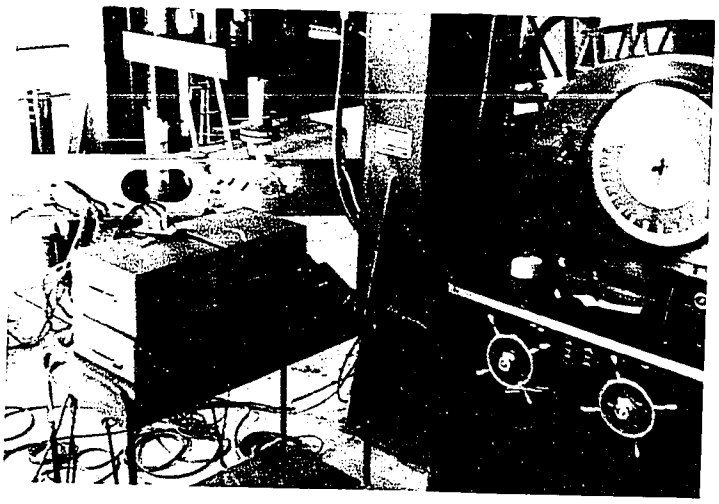

PLATE 4-3

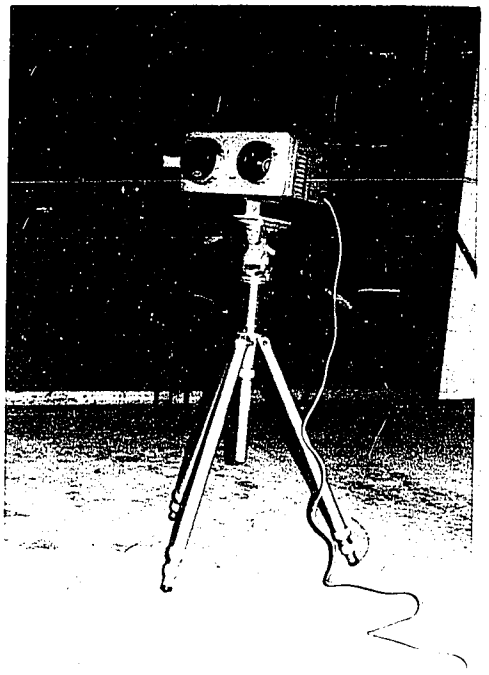

PLATE 4-4

λ = wave length of light corresponding to the retardation at the tint of passage (22.7×10^{-6} inches)

t_p = thickness of plastic sheet

K = strain-optical sensitivity of plastic sheet

F_c = reinforcement correction factor.

The values of K and t_p were supplied by the manufacturing company, and F_c can be found in the Chart shown in Appendix C.

Fringe orders were measured at the load of 40 kips for pure bending and at 10 kips for bending with shear. The measured points were selected slightly inside the boundary in order to avoid edge effects, and corrections were made in all tests by measuring the residual fringe orders due to absorption of moisture and other effects.

4.3 DEFLECTIONS AND ULTIMATE STRENGTH

Deflections were measured with 1/1000 inch dial gauges placed at two foot intervals along the span of the beam. Measurements were taken for each moment/shear ratio in the elastic range. In Tests Nos. 1 and 2, measurements were taken in 10 kip increments up to loads near the ultimate strength. Deflection readings were then discontinued and the loads were carried to failure.

To prevent lateral buckling, the compression flanges of both specimens were held by a lateral bracing system. No stiffeners were used under the loading point or at the reactions.

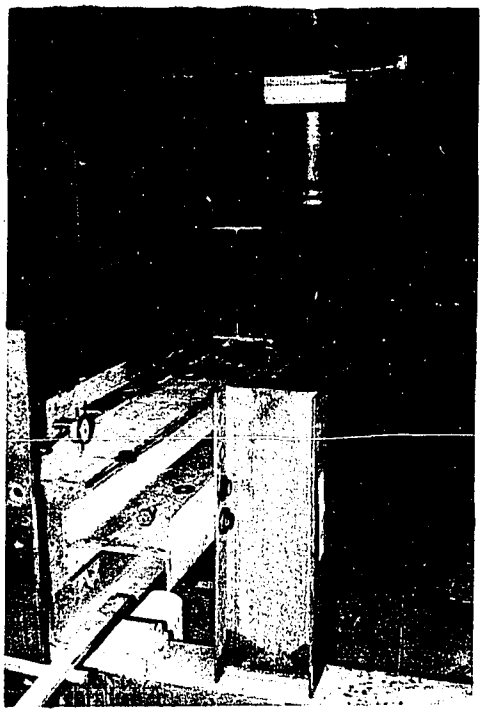

PLATE 4-5

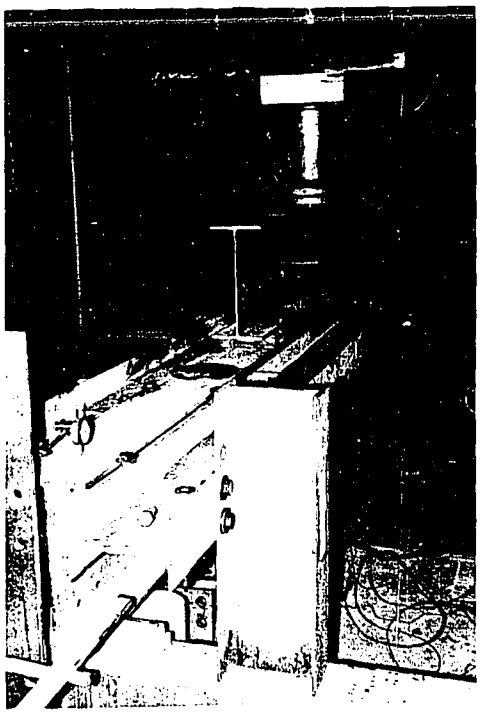

PLATE 4-5

CHAPTER V

INVESTIGATION OF THEORETICAL AND EXPERIMENTAL RESULTS

5.1 COMPARISON OF STRAIN GAUGE AND PHOTOSTRESS RESULTS

The strain gauge and photostress results are shown in Tables A.1 to A.11, Appendix A. The boundary stresses obtained from both methods are plotted in diagrams shown in Figures 5-1 to 5-4. The agreement between the two different approaches is good and only a single curve is drawn. When a discrepancy occurs, it is due to either a low strain level, or a steep strain gradient which makes the location of the reporting point critical.

5.2 COMPARISON OF EXPERIMENTAL AND THEORETICAL RESULTS

1. Elastic Behaviour

The theoretical results based on the methods mentioned in Chapter II are also plotted and compared with the experimental results in Figures 5-1 to 5-4. In the case of pure bending, the small hole theory[23] predicts well the stresses at the boundary of opening, with a deviation of about 5.8% at point of maximum stress, while the ring theory shows less accurate results, especially at the tangent point where the deviation is up to 31.7%.

The small hole theory predicts the stresses for the case of bending with shear very poorly, e.g. the deviation is as high as 55.6% at point of maximum stress for Test No. 2. However, the results

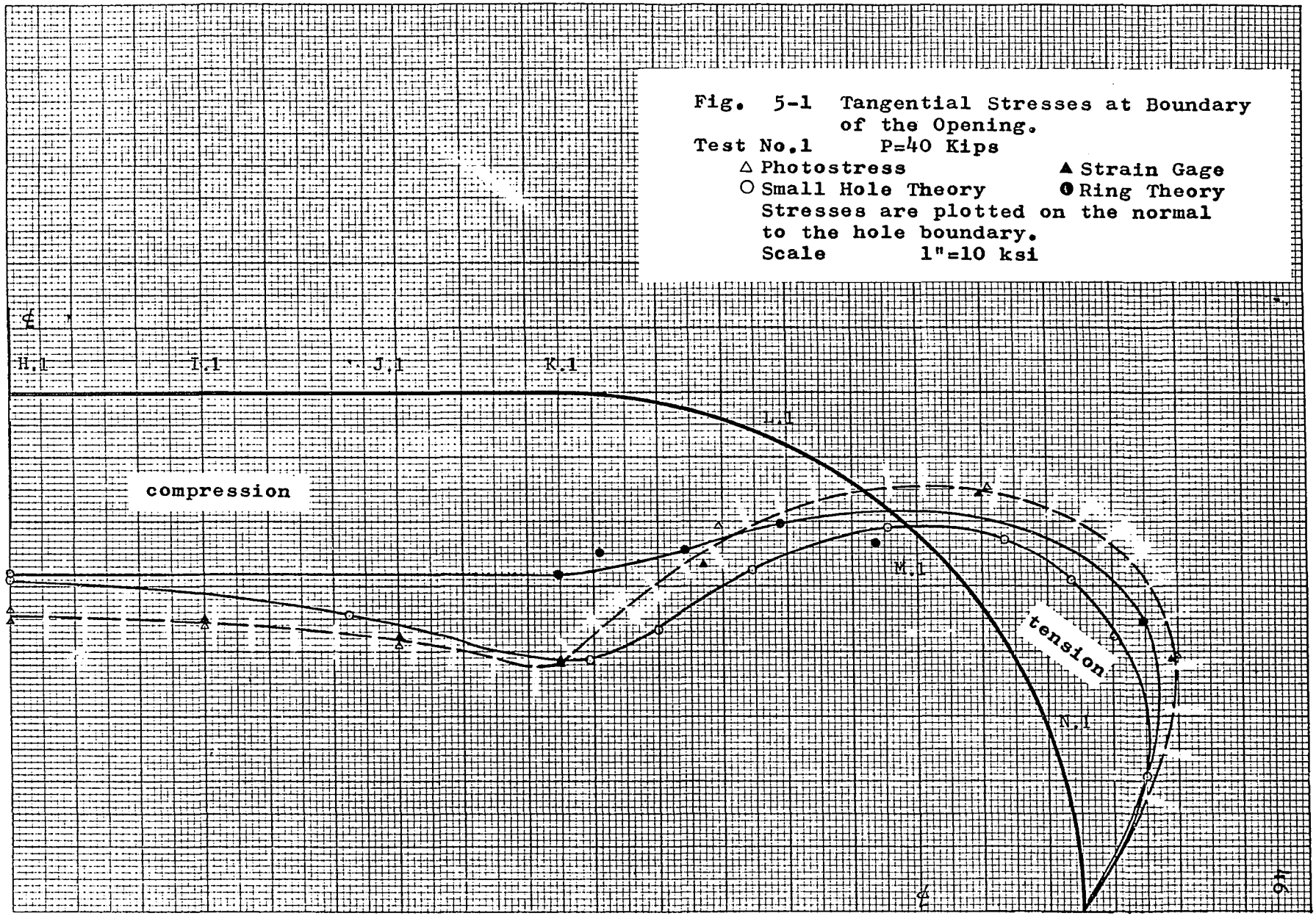

Fig. 5-1 Tangential Stresses at Boundary of the Opening.
Test No.1 P=40 Kips
△ Photostress ▲ Strain Gage
○ Small Hole Theory ● Ring Theory
Stresses are plotted on the normal to the hole boundary.
Scale 1"=10 ksi

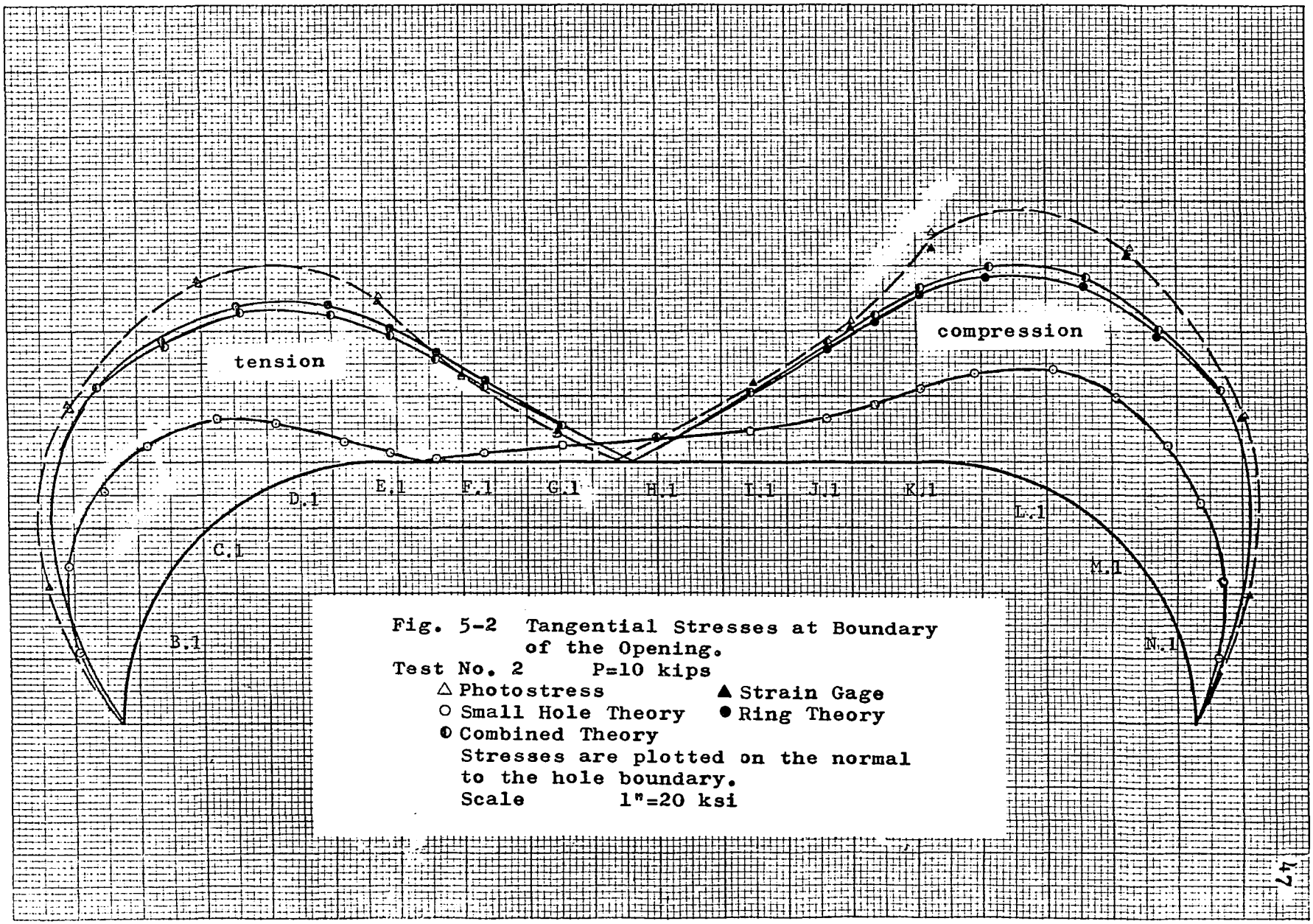

Fig. 5-2 Tangential Stresses at Boundary of the Opening.

Test No. 2 P=10 kips

△ Photostress ▲ Strain Gage

○ Small Hole Theory ● Ring Theory

◐ Combined Theory

Stresses are plotted on the normal to the hole boundary.

Scale 1"=20 ksi

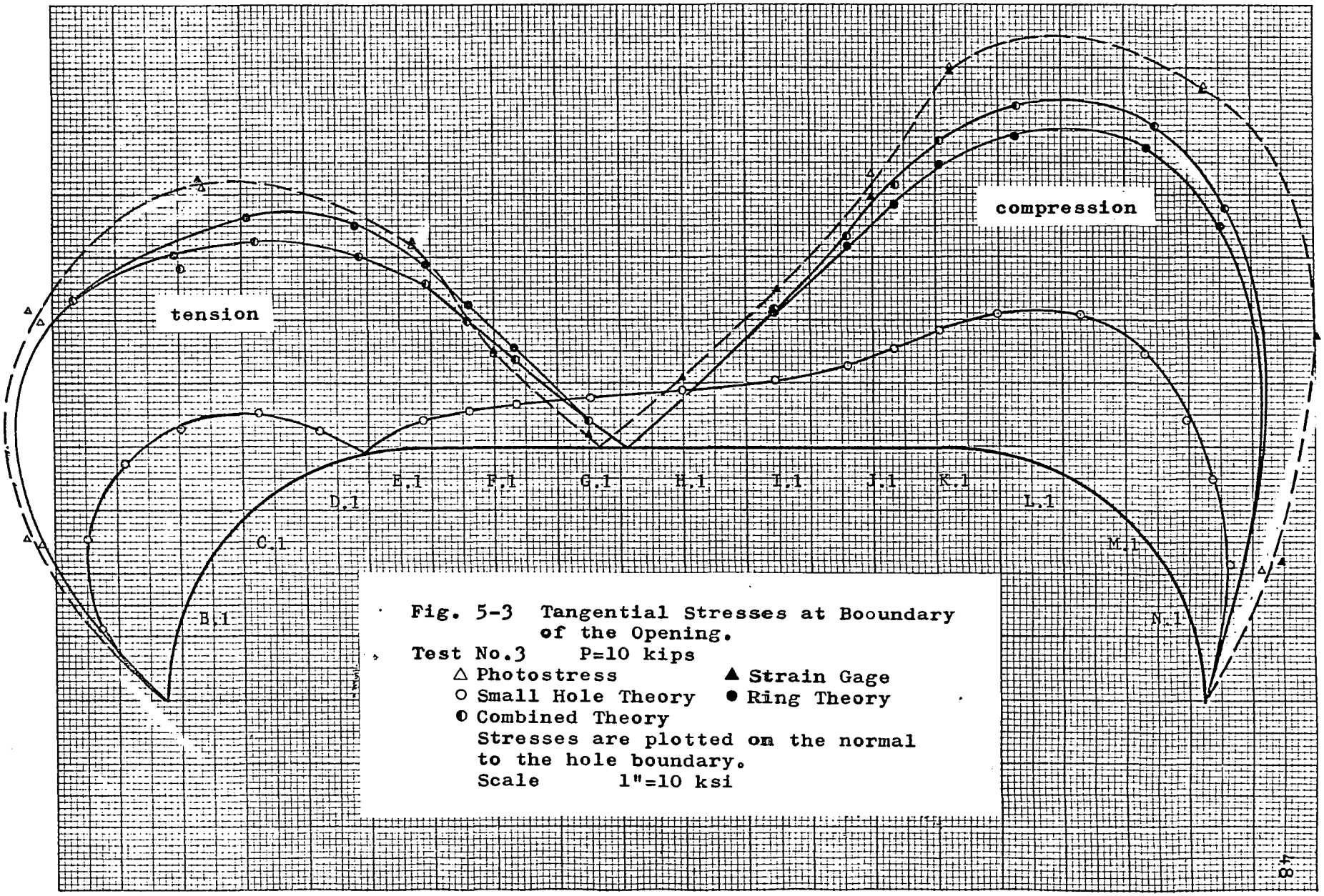

Fig. 5-3 Tangential Stresses at Boundary of the Opening.

Test No.3 P=10 kips

△ Photostress ▲ Strain Gage

○ Small Hole Theory ● Ring Theory

◐ Combined Theory

Stresses are plotted on the normal to the hole boundary.

Scale 1"=10 ksi

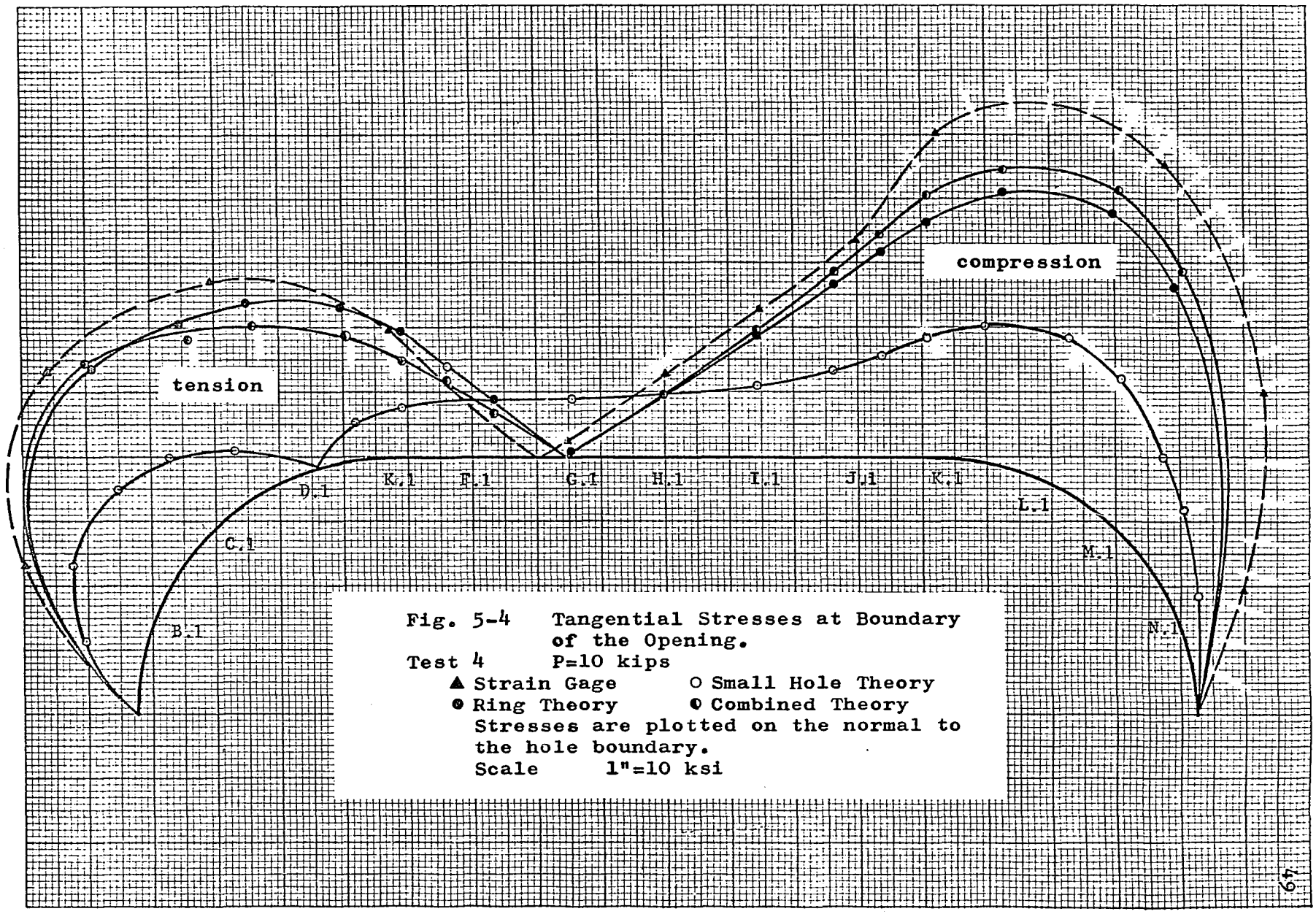

Fig. 5-4 Tangential Stresses at Boundary of the Opening.

Test 4 P=10 kips

▲ Strain Gage ○ Small Hole Theory

● Ring Theory ◐ Combined Theory

Stresses are plotted on the normal to the hole boundary.

Scale 1"=10 ksi

based on either ring or combined theory (i.e. small hole theory for pure bending plus ring theory for pure shear) shows a far more satisfactory agreement with the experimental results, especially the latter. This is due to the good accuracy of small hole theory for pure bending and that of ring theory for pure shear. The deviations at points of maximum stress, by results based on the combined theory, are a maximum of 17% for Tests Nos. 2 to 4.

In the case of pure bending, the applicability of small hole theory to a large opening even when its height is up to 57% of the beam depth is due to the following reason:

Figure 5-5a is a large plate (in two directions) with a small opening subjected to pure bending. The shear and the normal stresses on the sections $y = \pm h$, with approximately $y_o/h \leq 0.6$, are usually so small they can be neglected. This has been demonstrated by Tuzi[2] for the case of a circular opening. For a non-circular hole, these stresses could be found by modifying the solution developed by Heller et al.[23]. This is a lengthy procedure and the work involved was not considered justifiable. Intuitively, it is concluded that a similar state of stress distribution as in the case of a circular opening exists in the case of a non-circular opening. Therefore, the free body bounded by the lines $y = \pm h$ with loadings acting on both ends is identical to the element shown in Figure 5-5b. However, no such kind of identity exists in the case of pure shear, and thus the small hole theory tends to inaccurate results for the case of bending with shear.

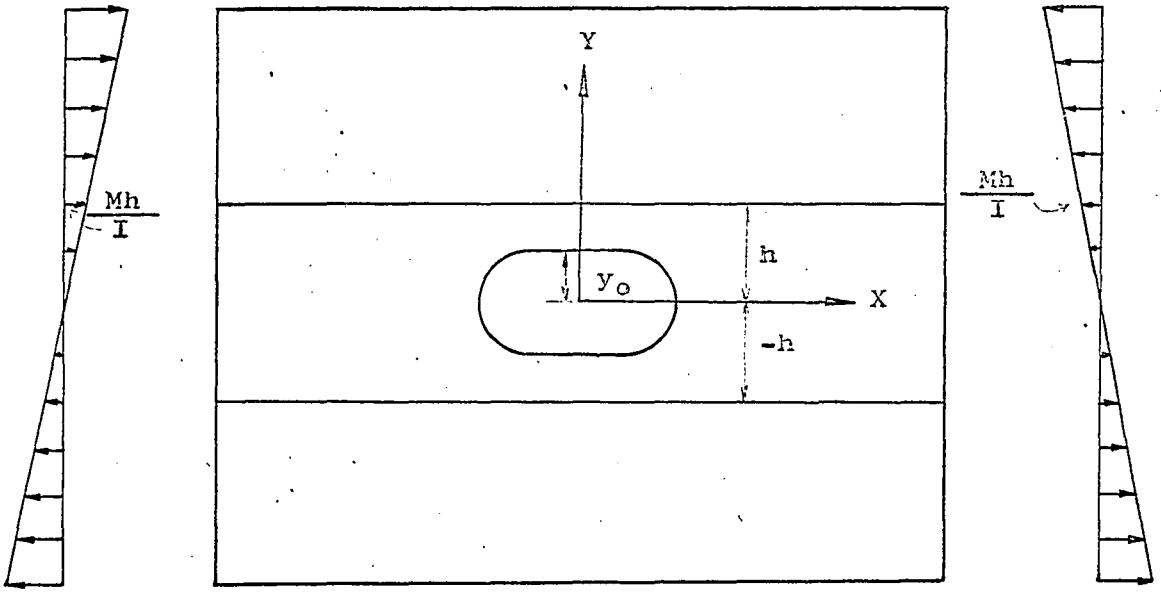

Fig. 5-5 (a)

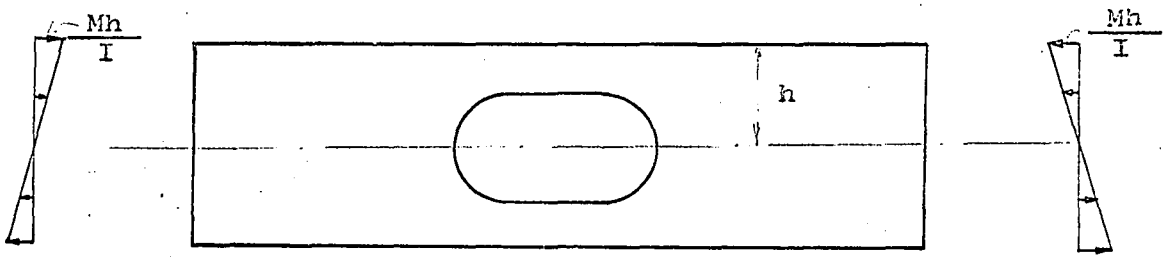

Fig. 5-5 (b)

The errors induced in the ring theory are mainly due to the simplifying assumption of plane sections remaining plane. The discrepancy can be clearly observed at the tangent point where a strain concentration exists due to the change of curvature of the bottom fiber of the tee.

2. Ultimate Strength

The theoretical and experimental results of the ultimate strength for Tests Nos. 1 and 2 are compared in Table 5-1. The theoretical values are calculated based on the methods developed in Chapter III. The deviation is 15.5% for pure bending and 13.8% for bending with shear (Test No. 2). The error of the former is possibly due to the non-uniform yield point stresses of the material of the wide-flange beam, and that of the latter is caused mainly by the assumption of ideally plastic material. As discussed in Chapter III, experiments have shown that the yield point stress of the flange can be considerably lower than that of the web. This will considerably reduce the plastic moment for the case of pure bending but not affect significantly the ultimate strength of the beam for the case of heavy ratio of shear to moment, since the moment arm of the flange forces is far larger for pure bending than for bending with shear (for a four plastic hinge mechanism). If an arbitrary ratio 1.3 of Y_w to Y_f is used and with Y_w remaining the smae as before, then the deviation becomes 5.8% for pure bending and 16.9% for Test No. 2. However, better results will be obtained for Test No. 2 if the effect of strain-hardening in the web near the boundary

TABLE 5-1

Comparison of Theoretical and Experimental Values of Ultimate Strength

	Test No. 1	Test No. 2
Experiment	75.9^{k}	35.5^{k}
Theoretical $\sigma_{y.p.} = 51$ ksi	90.5^{k}	30.6^{k} *
Error	+15.5%	-13.8%
Theoretical $Y_w = 51$ ksi, $Y_w/Y_f = 1.3$	71.5^{k}	29.5^{k}
Error	- 5.8%	-16.9%

* The calculation is based on Equation (3-9), i.e. the beam fails by a four hinge mechanism.

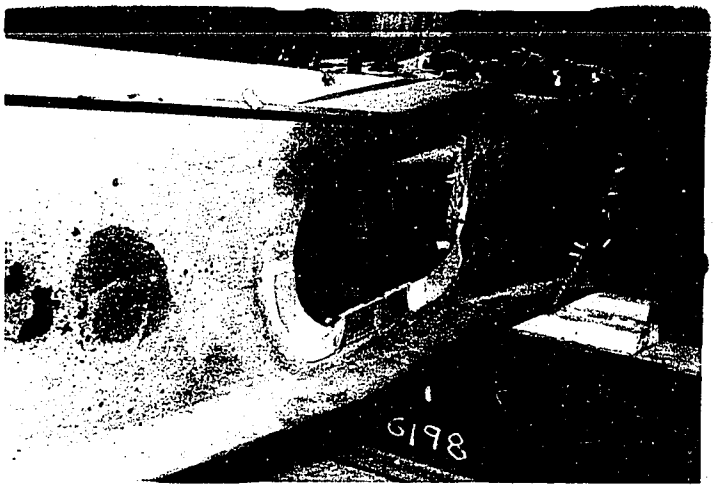

PLATE 5-1

PLATE 5-2

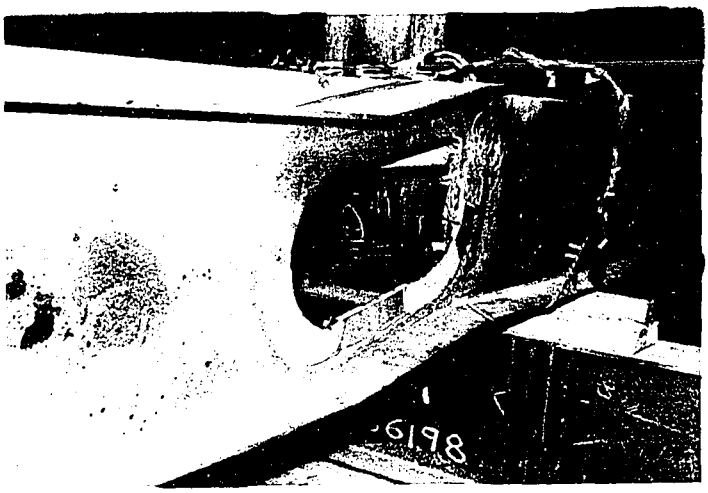

PLATE 5-1

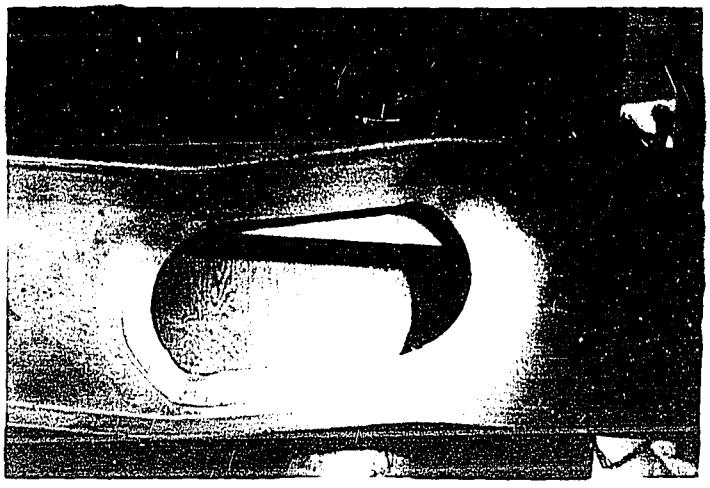

PLATE 5-2

is taken into consideration. In the experiment as shown in Plate 5-1, the beam seemed to fail by local buckling in the web as shown in Figure 3-3a.

5.3 CHARACTERISTICS OF ELASTIC AND PLASTIC BEHAVIOUR

1. Deflection

The measured deflections of the beam for different loading conditions and at various stages of loading are tabulated in Tables A.16 to A.19, Appendix A. Selected diagrams are plotted for deflections at some particular points for different stages of loading and for deflections of points of the whole span at various stages of loading. Some of the curves are compared with the theoretical value of the same beam without any opening subjected to the same loading condition, as shown in Figures 5-6 to 5-10. Additional deflections due to shear effect have been taken into consideration in the theoretical calculations. Typical calculations are shown in Appendix B.

For the case of pure bending, no significant difference occurs due to the presence of the opening. However, in the case of Test No. 2, the differences are up to 25% at the point of maximum deflection (point 4, as shown in Figure 5-10) and 35% at the point of maximum difference (point 2). These excess deflections are mainly due to the fact that the shear forces at the opening cause further relative deflection between two ends of the opening, as in the case of a rigid frame sideswaying under the action of transverse loading.

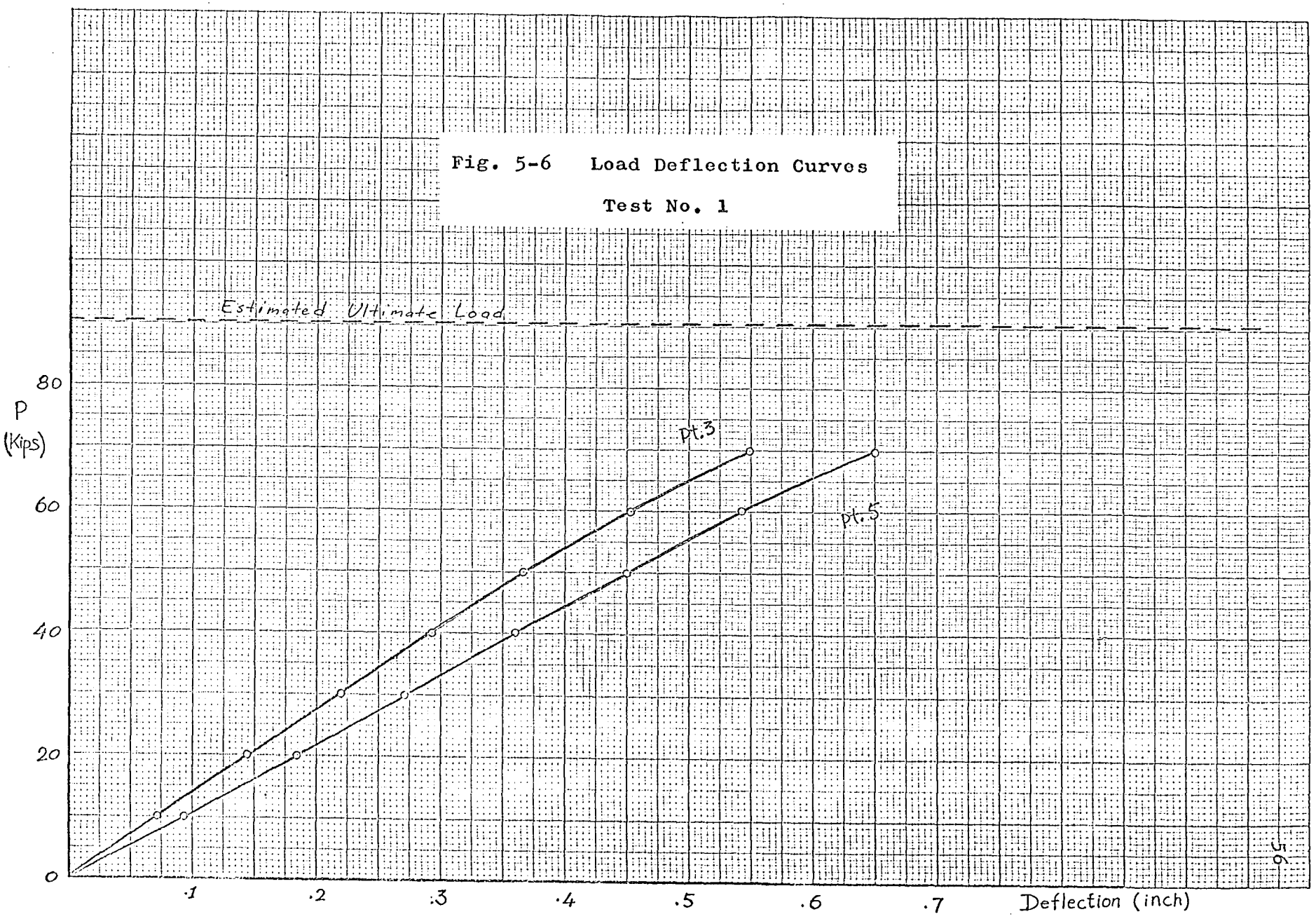

Fig. 5-6 Load Deflection Curves

Test No. 1

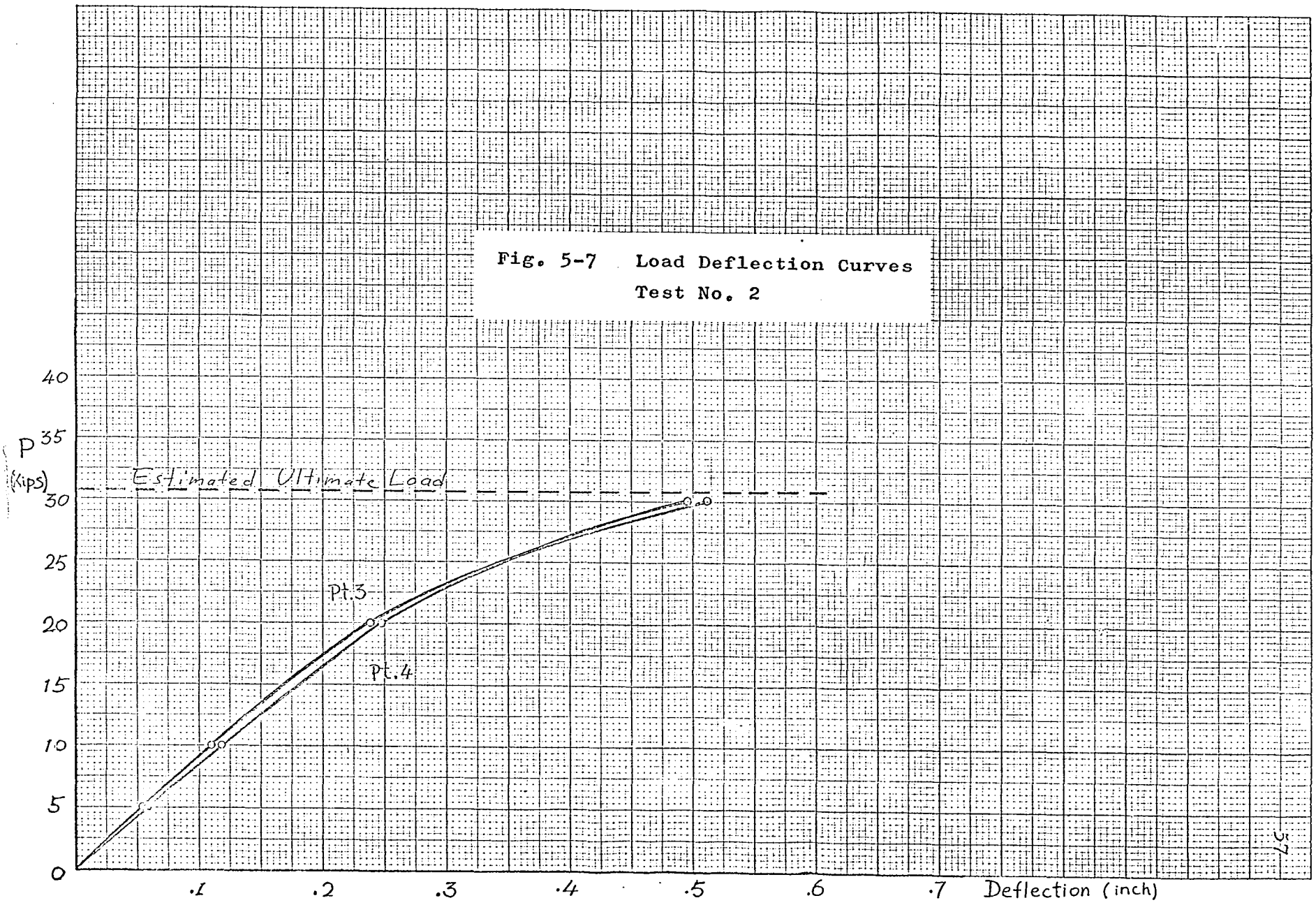

Fig. 5-7 Load Deflection Curves
Test No. 2

Fig. 5-8 Load Deflection Curves, Test No. 3

Full Lines- Measured Values
Broken Lines- Theoretical Values of Gross Section

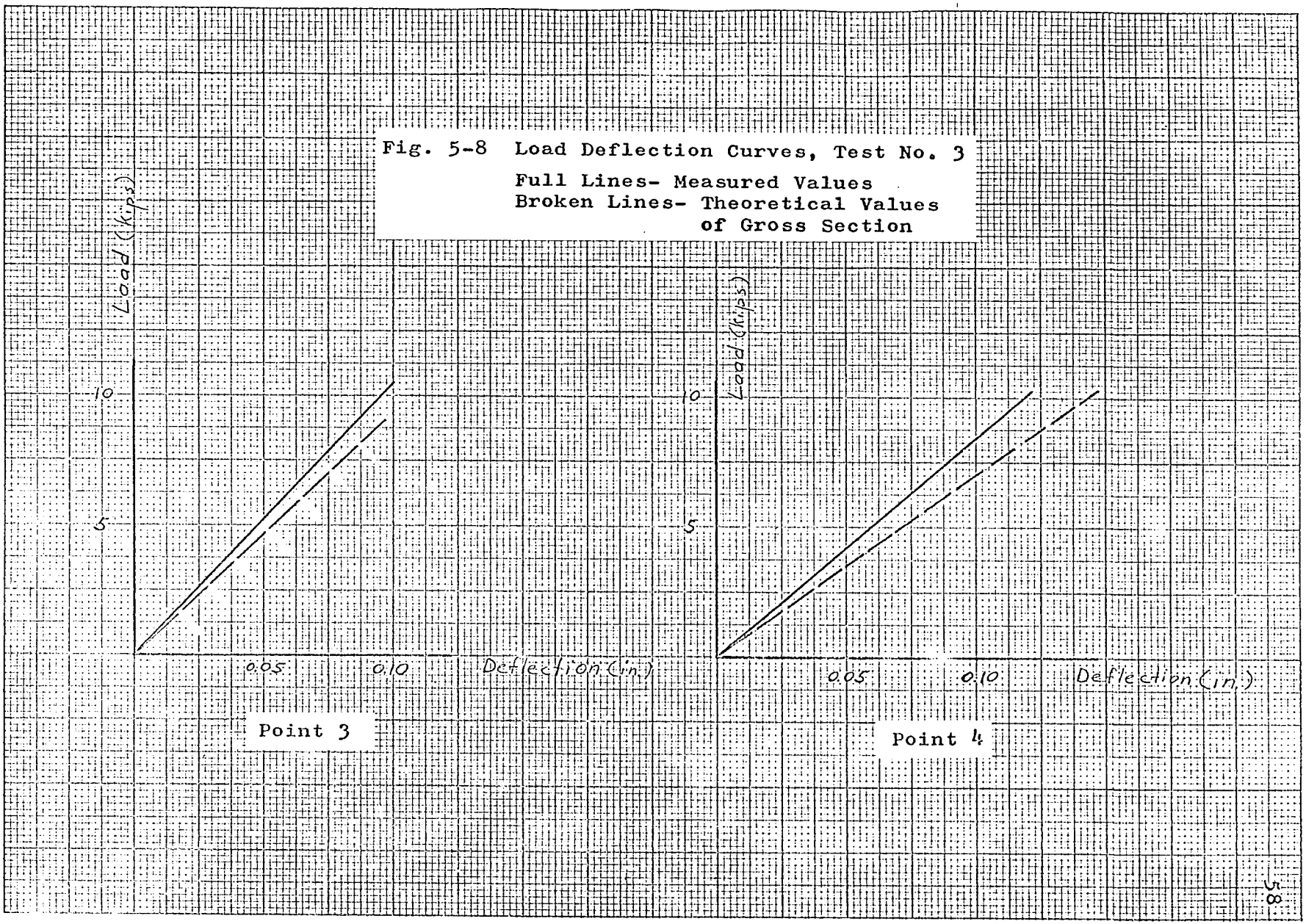

Fig. 5-9 Load Deflection Curves, Test No. 4

Full Lines- Measured Values
Broken Lines- Theoretical Values of Gross Section

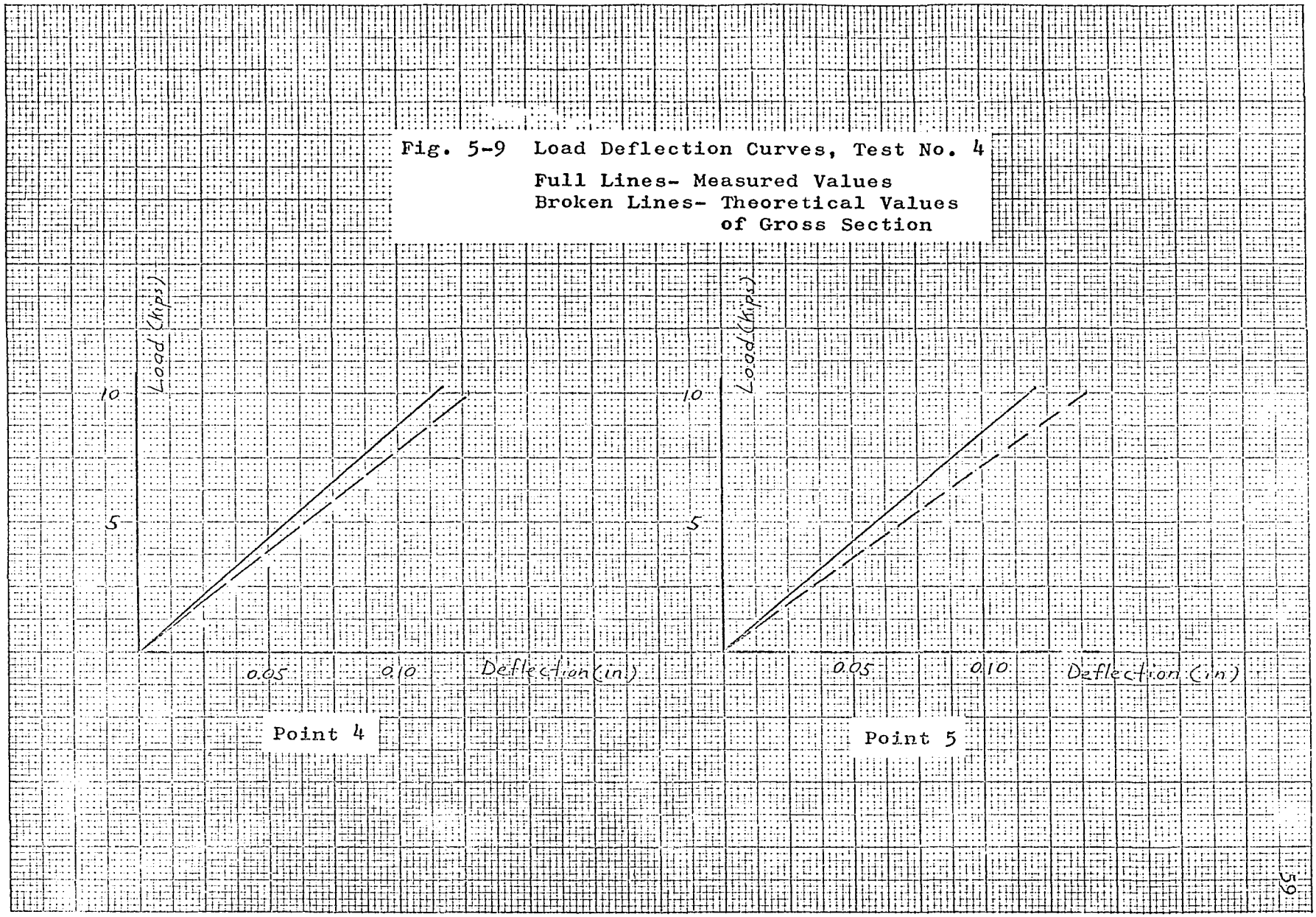

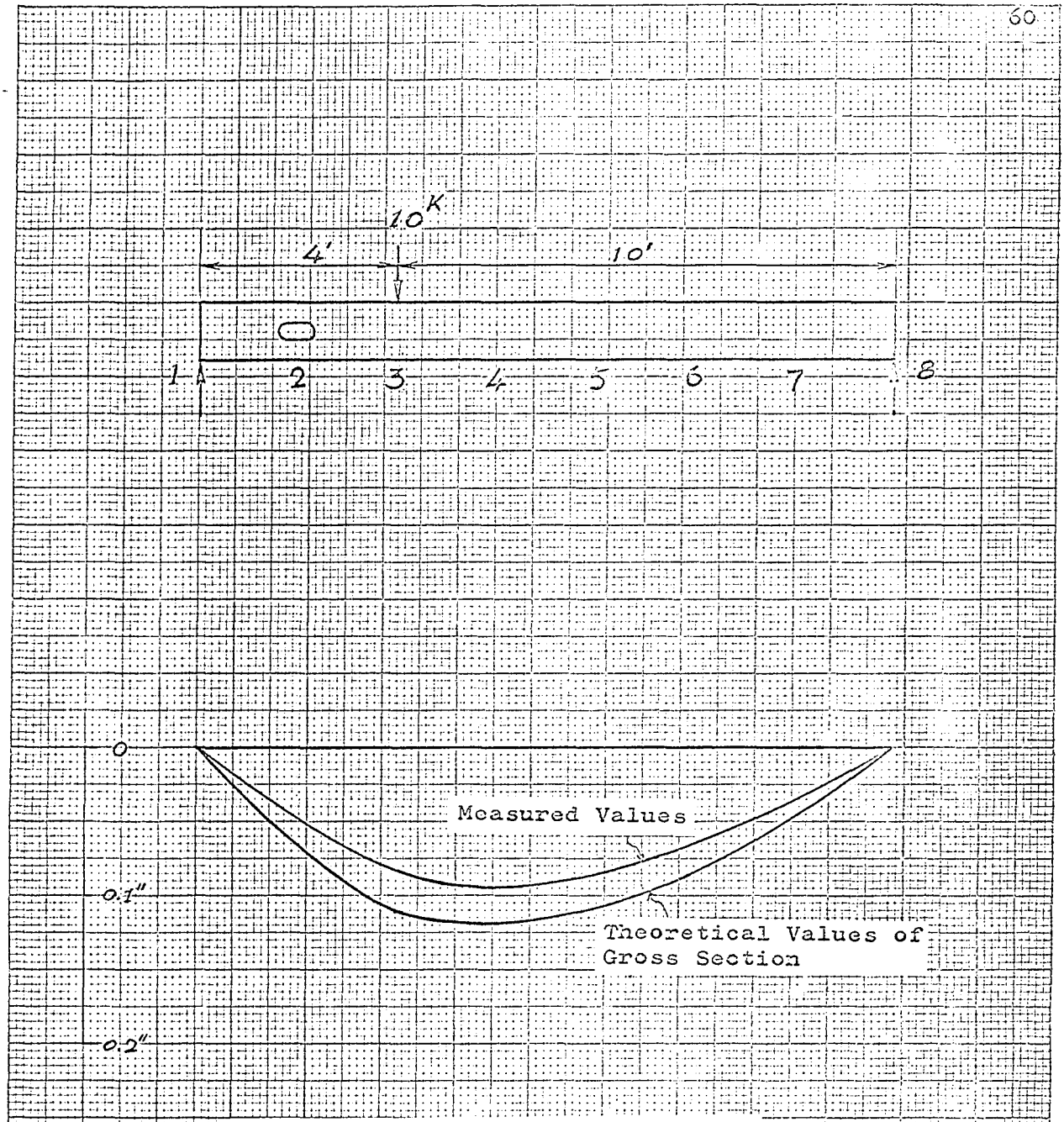

Fig. 5-10 Deflections of the Beam

2. Stress Distribution Shapes and Stress Concentration Factors

From the experimental results, selected curves indicating horizontal and vertical stress distributions in the region above (or below) the opening are shown in Figures 5-11 to 5-13. For the case of pure bending (Figure 5-13), the axial stresses at the sections near the centre of the opening are linearly (or approximately linearly) distributed along the vertical sections. An enlarged diagram indicating the stress distribution on the central section is shown in Figure 5-14 from which a good agreement between theoretical (based on Equation 2-2) and experimental results can be observed so long as the outside fiber stress of the flange is concerned. The stress concentration factor is calculated to be 1.05 with critical stress occurring at the outside fiber of the flange. Here the stress concentration factor F is defined as

$$F = \frac{\sigma_{max}}{\sigma_{nom}}$$

with σ_{nom} (nominal stress) = M/Z, where M is the moment at the central line of the opening and Z the section modulus of the same beam without any opening. It is worth repeating that the maximum stress for pure bending is not on the boundary of the opening but at the outside fiber of the flange. In Test No. 2, no linear stress distribution along the vertical sections exists as in the case of pure bending. A steep stress gradient occurs at the section where the depth of the web begins to change. The stress concentration factor (as defined before) for Test No.

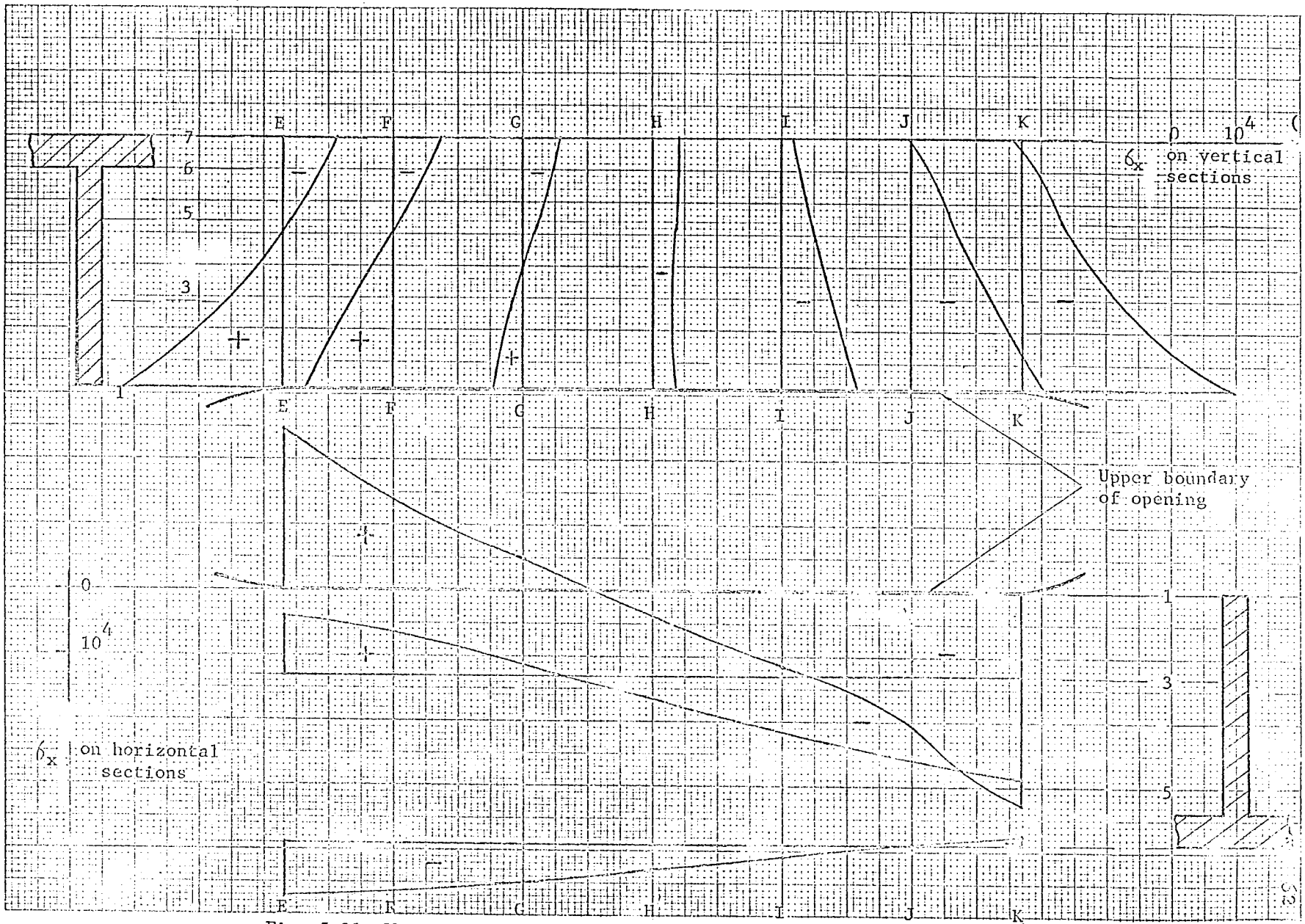

Fig. 5-11 Vertical and Horizontal Stress Distributions, Test No. 2 P=10 kips

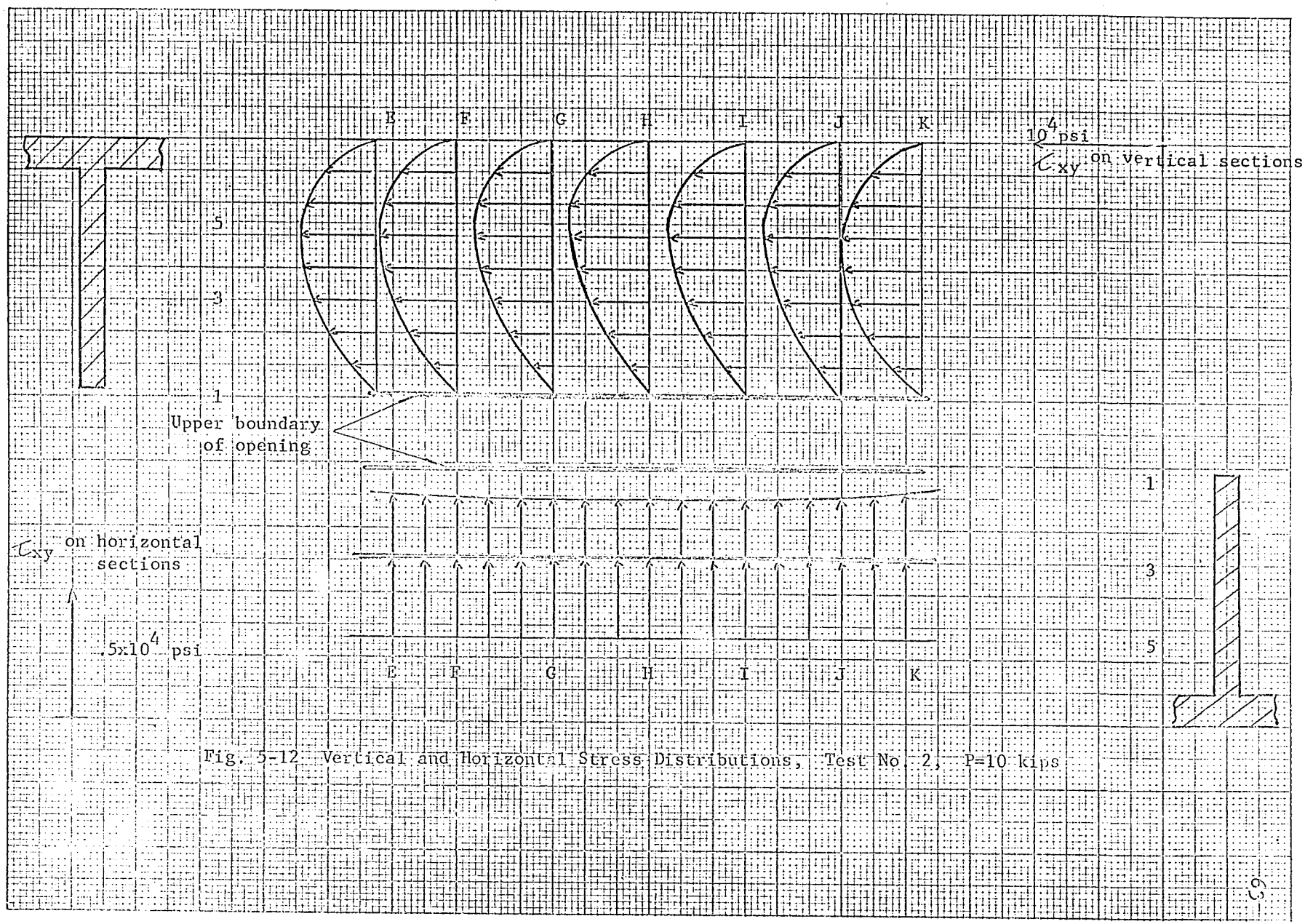

Fig. 5-12 Vertical and Horizontal Stress Distributions, Test No. 2, P=10 kips

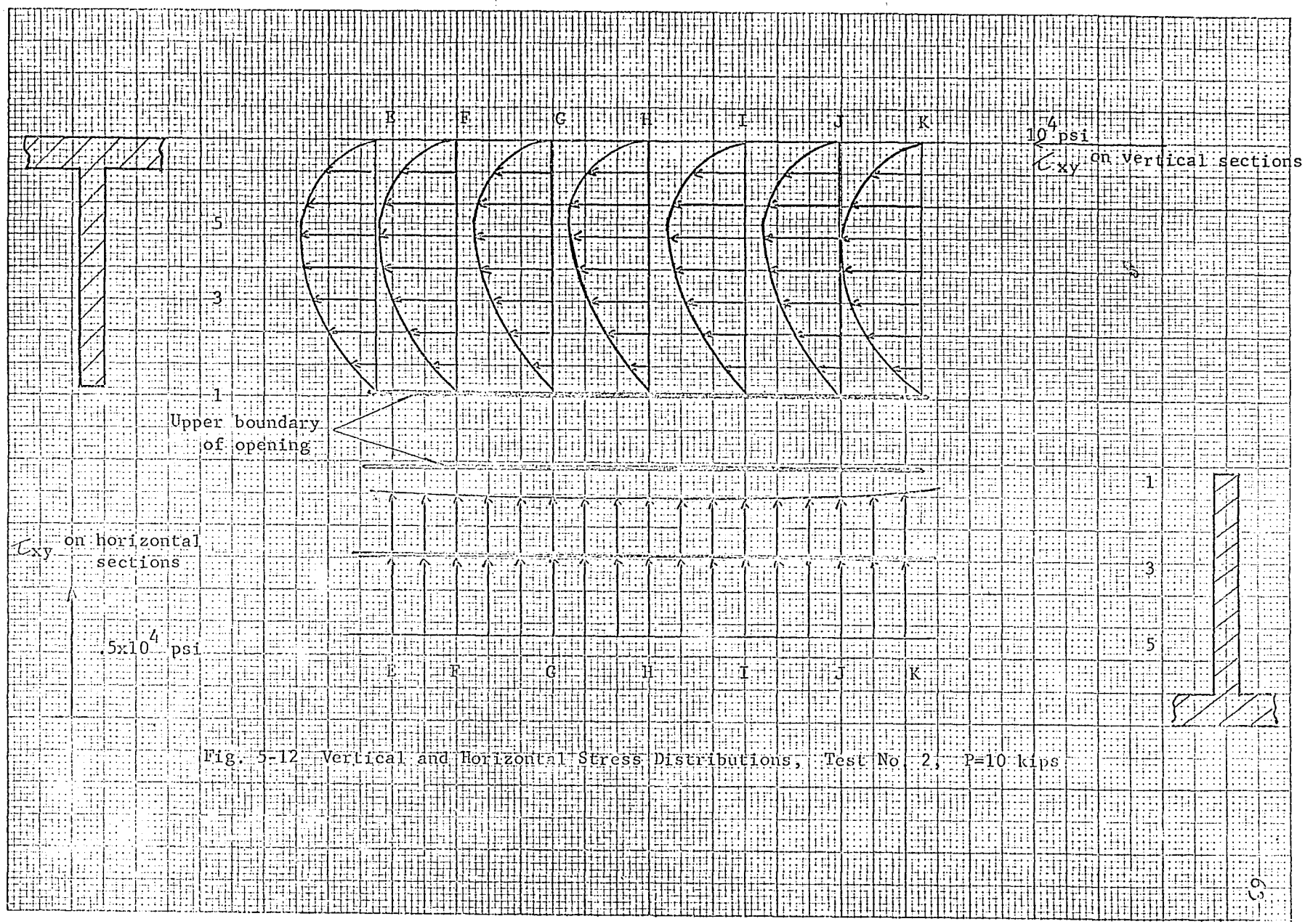

Fig. 5-12 Vertical and Horizontal Stress Distributions, Test No. 2, P=10 kips

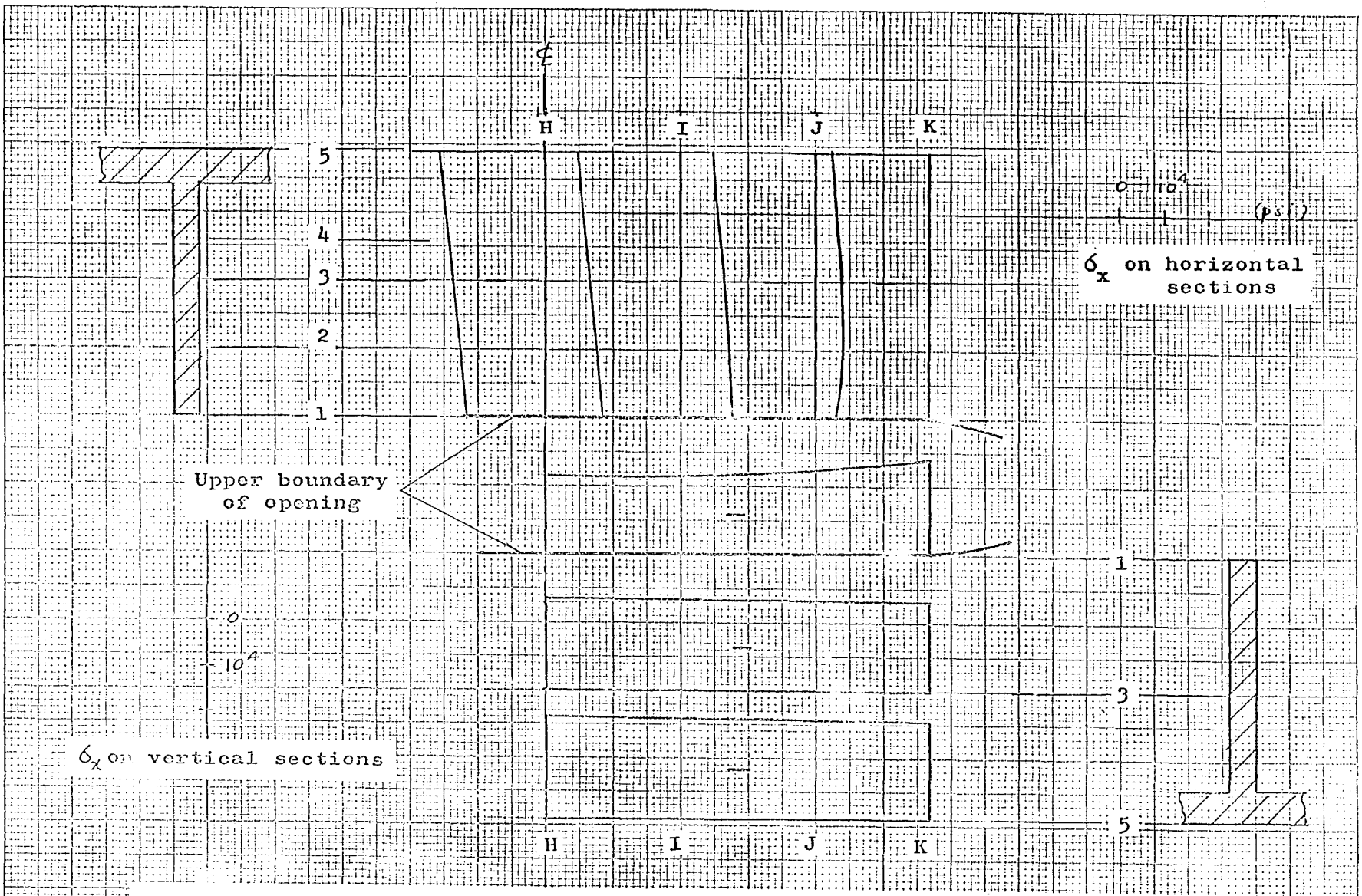

Fig. 5-13 Vertical and Horizontal Stress Distribution, Test No. 1, P=40 kips

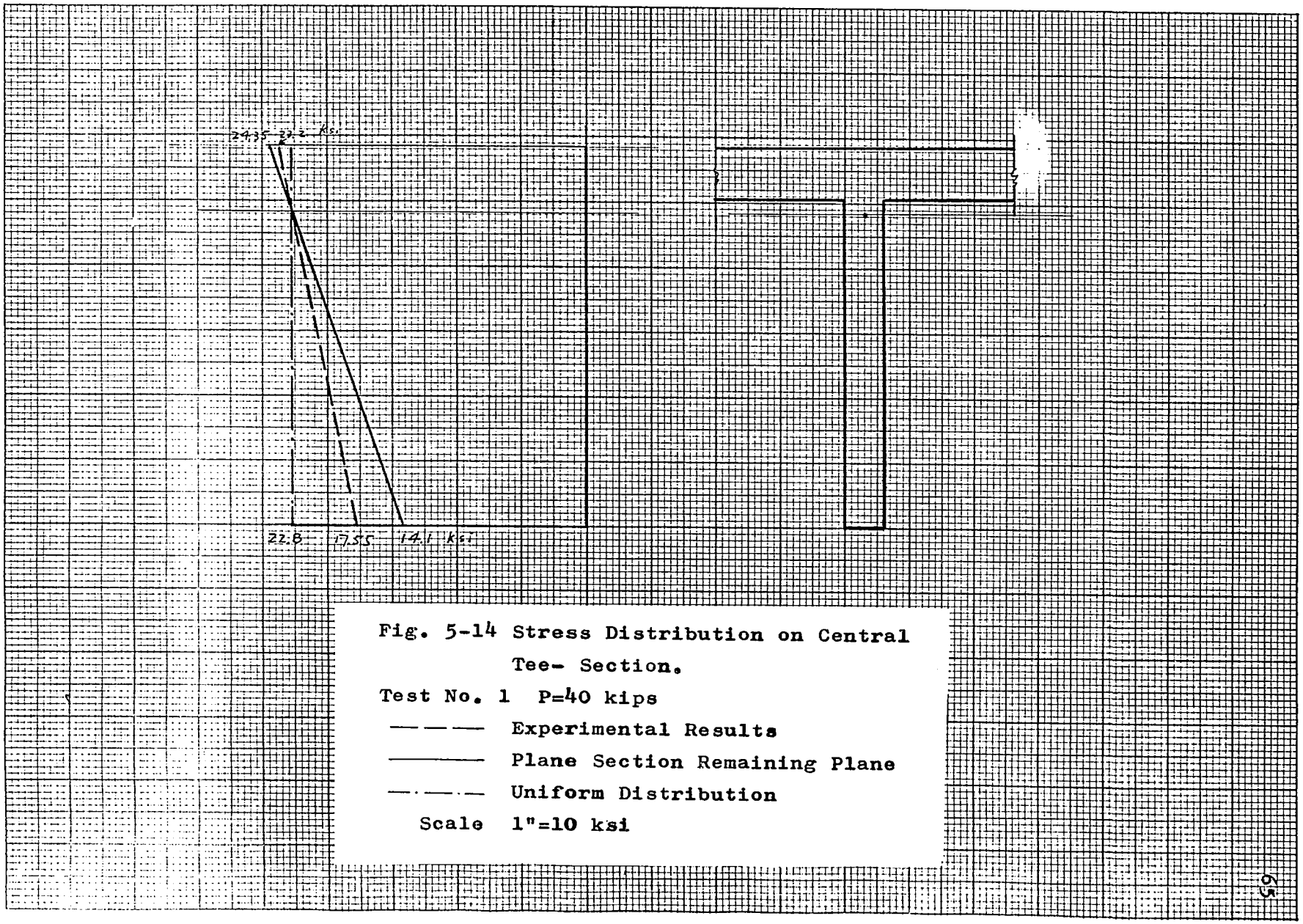

Fig. 5-14 Stress Distribution on Central Tee- Section.

Test No. 1 P=40 kips

——— Experimental Results

——————— Plane Section Remaining Plane

—·——·— Uniform Distribution

Scale 1"=10 ksi

2 is calculated to be 9.37 and those for Tests Nos. 3 and 4 are 4.94 and 3.55 respectively. All the maximum stresses occur at the boundary of the opening, somewhere near the tangent point on the half-circular portion.

3. Ultimate Strength

The reductions of ultimate strength due to the presence of opening are calculated theoretically as 9.5% in pure bending, 56.2% in Test No. 2, 28.3% in Test No. 3, and 22.8% in Test No. 4, while experiments showed 24.5% in pure bending and 49.4% in Test No. 2. This data indicates that the shear is a significant factor in reducing ultimate strength of the beam with an extended opening in the web, especially when the horizontal length of the opening is long.

CHAPTER VI

CONCLUSIONS

The following conclusions can be drawn:

1. In the case of pure bending, the theory of elasticity with the assumption that the hole is small predicts well the elastic stresses at the boundary of the opening even when its height is up to 57% of beam depth. For the size and shape of the opening tested experimentally the stress concentration factor is 1.05 with the critical stress occurring at the outside fiber of the flange. Hence, for elastic analysis, the effect of the opening can be neglected.

2. In the case of bending with shear, the combined theory (i.e, small hole theory for pure bending plus ring theory for pure shear) predicts the stresses at the boundary of the opening with a maximum error of about 17% for the size and shape of the opening tested experimentally.

3. The critical stress for all cases of bending with shear occurs at the boundary of the openings, somewhere near the tangent point on the semi-circular portion. The stress concentration factors are 9.37 for Test 2, 4.94 for Test 3 and 3.55 for Test 4. Hence, for elastic analysis, the effect of the opening cannot be neglected under these conditions.

4. The lower bound solutions for the ultimate strength are given in general forms and are applicable to various shapes of opening.

The solution satisfactorily predicts the strength of the one experimental test for bending with shear. Further experimental evidence is required in order to establish more general validity.

5. The failure moment at the opening in Test 2 is 0.33 of the failure moment under pure bending. This significant reduction in moment capacity due to the presence of shear indicates that reinforcement of the opening must be considered under these conditions.

6. For the case of pure bending, no significant difference in deflection occurs due to presence of the opening. However, the difference is large for bending with shear and is up to 25% at the point of maximum deflection in Test No. 2.

APPENDIX A

EXPERIMENTAL AND THEORETICAL DATA

TABLE A.1

Comparison of Strain Gauge and Photostress Results

Position	Value $e_t \times 10^6$ S.G.	$e_t \times 10^6$ P.S.	σ_t (psi) S.G.	σ_t (psi) P.S.	% Variation from mean
H.1	-585	-568	-17550	-17050	1.4
I.1	-585	-608	-17550	-18230	2.0
J.1	-632	-656	-18970	-19700	1.9
K.1	-704	-696	-21000	-20900	0.6
L.1	-381	-275	-11430	- 8250	16.2
M.1	185	203	5550	6090	4.6
N.1	354	404	10620	12110	6.6

[Test No. 1: P = 40 kips]

TABLE A.2

Comparison of Strain Gauge and Photostress Results

Position	Value $e_t \times 10^6$ S.G.	$e_t \times 10^6$ P.S.	σ_t (psi) S.G.	σ_t (psi) P.S.	% Variation from mean
B.1	501	503	15020	15090	0.2
C.1	936	915	28100	27450	1.2
D.1	1104	1078	33150	32320	3.2
E.1	820	844	24600	25300	1.4
F.1	454	429	13620	12880	2.7
G.1	160	138	4800	4140	7.4
H.1	- 120	-	- 3800	-	-
I.1	- 394	- 405	-11820	-12160	1.5
J.1	- 690	- 721	-20700	-21650	2.0
K.1	-1094	-1167	-32820	-35000	3.2
L.1	-1260	-1300	-37800	-39000	1.6
M.1	- 889	- 907	-26650	-27200	1.0
N.1	- 408	- 389	-12240	-11980	2.3

[Test No. 2: P = 10 kips]

Note: Refer to Figures 4-3 and 4-4 for identification of strain gauge locations.

TABLE A.3

Comparison of Strain Gauge and Photostress Results

Position	Value $e_t \times 10^6$ S.G.	$e_t \times 10^6$ P.S.	σ_t (psi) S.G.	σ_t (psi) P.S.	% Variation from mean
B.1	439	397	13180	11910	5.0
C.1	767	729	23080	21880	2.5
D.1	816	794	24520	23800	1.4
E.1	544	535	16320	16050	0.7
F.1	252	243	7560	7300	1.6
G.1	32	-	960	-	-
H.1	- 188	- 186	- 5640	- 5580	0.5
I.1	- 412	- 413	-12360	-12400	0.1
J.1	- 660	- 720	-19800	-21600	4.3
K.1	- 990	-1000	-29700	-30000	0.5
L.1	-1079	-1085	-32370	-32600	0.3
M.1	- 693	- 690	-20800	-20700	0.2
N.1	- 281	- 227	- 8430	- 6820	10.6

[Test No. 3: P = 10 kips]

TABLE A.4

Tangential Strains and Stresses

Position	Value $e_t \times 10^6$ S.G.	σ_t (psi)
B.1	353	10600
C.1	592	17800
D.1	551	16550
N.1	-187	- 5600
M.1	-520	-15600
L.1	-874	-26200

[Test No. 4: P = 10 kips]

TABLE A.5

Strain Gauge Results and Derived Stresses in Cartesian Coordinates

(The x-Axis is the Longitudinal Axis of the Beam)

Position	Value	$e_x \times 10^6$	$e_y \times 10^6$	$e_{xy} \times 10^6$	σ_x (psi)	σ_y (psi)	τ_{xy} (psi)
H.1		-585	146	0	-17550	0	0
H.2		-637	163	21	-19080	120	249
H.3		-695	179	20	-20807	168	235
H.4		-718	191	- 3	-21451	337	- 42
I.1		-585	146	0	-17550	0	0
I.2		-635	166	- 14	-18989	3	69
I.3		-675	184	48	-20130	477	582
J.1		-632	158	0	-18970	0	0
J.2		-633	158	8	-18989	243	- 166
J.3		-688	173	14	-20629	43	166
J.4		-718	184	1	-21504	144	14
K.1		-704	176	0	-21000	0	0
K.2		-631	128	44	-19171	- 963	527
K.3		-648	154	- 8	-19503	- 256	- 97
L.2		-501	118	44	-15085	- 222	533
L.3		-588	184	- 57	-17359	1172	- 689
L.4		-682	191	-111	-20293	667	-1330
M.2		-208	131	21	- 5607	2540	256
M.3		-325	159	87	- 9139	2473	1048
M.4		-656	169	70	-19624	149	845
N.2		- 6	96	-145	559	3014	-1737
N.3		- 58	49	- 84	- 1453	1107	1005
F.5		-760			-22800		
H.5		-775			-23250		
J.5		-750			-22500		
L.5		-720			-21600		

[Test No. 1: P = 40 kips]

TABLE A.6

Strain Gauge Results and Derived Stresses in Cartesian Coordinates

Position	Value	$e_x \times 10^6$	$e_y \times 10^6$	$e_{xy} \times 10^6$	σ_x (psi)	σ_y (psi)	τ_{xy} (psi)
B.2		145	104	441	5460	4487	5295
B.4		193	- 21	390	6013	867	4677
C.2		373	88	495	12636	5791	5944
C.4		274	- 2	127	8765	2142	1528
C.5		- 100	31	178	- 2955	181	2134
D.2		465	25	410	15092	4534	4926
D.4		189	57	180	6493	3347	2161
D.5		- 70	61	147	- 1749	1403	1760
E.1		820	-205	0	24600	0	0
E.3		277	- 14	406	8754	1779	4877
F.1		454	-112	0	13620	0	0
F.3		210	- 42	358	6384	336	-4295
F.5		- 43	20	506	- 1219	285	6069
G.1		160	- 40	0	4800	0	0
G.3		50	3	370	1573	293	4434
H.1		- 120	30	0	- 2800	0	0
H.3		- 116	53	366	- 3290	757	4392
H.5		- 128	43	517	- 3755	341	6208
I.1		- 394	98	0	-11820	0	0
I.3		- 394	125	370	-11610	837	4434
J.1		- 690	172	0	-20700	0	0
J.3		- 426	127	367	-12613	667	4406
J.5		- 218	49	510	- 6587	- 187	6125
K.1		-1094	273	0	-32820	0	0
K.3		- 510	70	457	-15760	-1840	5487
L.2		- 617	20	485	-19584	-4309	5815
L.4		- 386	6	188	-12304	-2896	2254
L.5		- 196	2	137	- 6256	-1504	1649
M.2		- 397	- 85	591	-13368	-5885	7088
M.4		- 370	46	227	-11455	-1478	2720
M.5		- 133	54	-147	- 3821	675	-1760
N.2		- 141	-111	431	- 5393	-4687	5172
N.4		- 182	18	369	- 5671	- 889	4428

[Test No. 2: P = 10 kips]

TABLE A.7

Strain Gauge Results and Derived Stresses

in Cartesian Coordinates

Position	Value $e_x \times 10^6$	$e_y \times 10^6$	$e_{xy} \times 10^6$	σ_x (psi)	σ_y (psi)	τ_{xy} (psi)
C.6	- 220	53	- 46	- 6,613	- 53	- 554
C.7	- 298	92	- 45	- 8,800	560	- 540
D.6	- 185	71	39	- 5,352	792	471
D.7	- 374	111	23	-11,077	571	277
F.6	- 165	144	- 1	- 4,131	3,277	- 14
F.7	- 268	85	104	- 7,893	587	1,247
H.6	- 140	38	165	- 4,176	96	1,981
H.7	- 136	43	121	- 4,005	299	1,455
J.6	- 110	14	122	- 3,408	- 432	1,469
J.7	4	7	106	181	245	1,275
L.6	- 88	1	30	- 2,805	- 661	360
L.7	80	- 21	43	2,395	- 21	513
M.6	- 54	23	- 28	- 1,541	315	- 333
M.7	- 16	- 8	- 32	- 576	- 384	- 388

Test No. 2: P = 10 kips

TABLE A.8

Strain Gauge Results and Derived Stresses in Cartesian Coordinates

Position	Value	$e_x \times 10^6$	$e_y \times 10^6$	$e_{xy} \times 10^6$	σ_x (psi)	σ_y (psi)	τ_{xy} (psi)
B.2		154	- 22	317	4750	830	3808
B.4		116	94	376	4450	3923	4518
C.2		392	- 39	-121	12238	1896	-1454
C.4		196	7	29	6326	1781	352
C.5		-196	54	158	- 5840	160	1898
D.2		298	37	321	9821	3566	5853
D.4		55	68	140	2290	2616	1679
D.5		-164	69	127	- 4693	907	1524
E.1		544	-136	0	16320	0	0
E.3		115	9	324	3752	1208	3894
F.1		252	- 63	0	7560	0	0
F.3		66	- 15	299	1995	59	3589
F.5		-145	38	395	- 4339	45	4739
G.1		32	- 8	0	960	0	0
G.3		- 60	24	303	- 1728	288	3630
H.1		-188	47	0	- 5640	0	0
H.3		-194	68	294	- 5664	624	3533
H.5		-210	56	401	- 6272	112	4808
I.1		-412	103	0	-12360	0	0
I.3		-314	97	298	- 9275	581	3575
J.1		-660	165	0	-19800	0	0
J.3		-450	152	260	-13184	1264	3118
J.5		-286	63	405	- 8651	- 283	4864
K.1		-990	247	0	-29700	0	0
K.3		-500	71	379	-13435	-1739	4545
L.2		-576	38	395	-18139	-3408	4740
L.4		-401	30	147	-12591	-2235	1768
L.5		-265	33	105	- 8216	-1064	1261
M.2		-363	- 17	520	-11757	-3443	6240
M.4		-352	53	199	-10837	-1110	2392
M.5		209	70	- 99	- 6131	557	-1192
N.2		-104	- 80	312	- 3967	-3392	3749
N.4		-159	14	290	- 4988	- 825	3484

[Test No. 3: P = 10 kips]

TABLE A.9

Strain Gauge Results and Derived Stresses

in Cartesian Coordinates

Position	$e_x \times 10^6$	$e_y \times 10^6$	$e_{xy} \times 10^6$	σ_x (psi)	σ_y (psi)	τ_{xy} (psi)
Value						
C.6	- 284	81	- 57	- 8443	309	- 679
C.7	- 366	108	- 57	-10848	528	- 679
D.6	- 255	94	30	- 7405	979	360
D.7	- 429	125	31	-12728	568	374
F.6	- 238	88	128	- 6912	912	1538
F.7	- 337	96	88	-10013	387	1053
H.6	- 224	71	121	- 6597	491	1454
H.7	- 230	63	92	- 6853	187	1109
J.6	- 204	55	105	- 6085	139	1261
J.7	- 120	33	91	- 3579	85	1095
L.6	- 186	31	16	- 5701	- 485	194
L.7	- 56	21	24	- 1627	213	291
M.6	- 160	53	- 35	- 4693	427	- 416
M.7	- 130	33	- 17	- 3893	27	- 208

Test No. 3: P = 10 kips

TABLE A.10

Strain Gauge Results and Derived Stresses in Cartesian Coordinates

Position	Value	$e_x \times 10^6$	$e_y \times 10^6$	$e_{xy} \times 10^6$	σ_x (psi)	σ_y (psi)	τ_{xy} (psi)
B.2		99	- 13	252	3075	391	3028
B.4		86	63	307	3244	2703	3688
C.2		287	- 40	- 63	8859	1007	- 753
C.4		123	11	- 7	4011	1323	- 88
C.5		-232	59	130	- 6949	43	1566
D.2		147	38	234	5021	2392	2804
D.4		- 25	76	117	- 194	2221	1399
D.5		-210	69	98	- 6165	539	1178
E.1		326	- 81	0	9780	0	0
E.3		7	20	226	387	707	2716
F.1		126	- 31	0	3780	0	0
F.3		- 30	3	219	- 933	- 133	2633
F.5		-196	46	304	- 5904	- 96	3644
G.1		- 45	11	0	- 1350	0	0
G.3		-120	41	232	- 3515	341	2633
H.1		-218	54	0	- 6540	0	0
H.3		-255	68	219	- 6653	387	2633
H.5		-248	64	309	- 7424	64	3713
I.1		-380	95	0	-11400	0	0
I.3		-320	89	212	- 9525	299	2550
J.1		-562	140	0	-16860	0	0
J.3		-412	113	216	-12283	309	2591
J.5		-295	62	328	- 8941	- 365	3935
K.1		-838	209	0	-25140	0	0
K.3		-448	59	290	-13861	-1685	3478
L.2		-490	38	300	-15392	-2715	3595
L.4		-374	40	104	-11637	-1723	1254
L.5		-285	37	70	- 8824	-1096	845
M.2		-294	- 32	374	- 9665	-3375	4488
M.4		-305	55	156	- 9323	- 677	1872
M.5		-244	64	- 69	- 7296	96	- 831
N.2		- 89	- 66	222	- 3364	-2823	2669
N.4		-131	8	208	- 4141	- 793	2500

[Test No. 4: P = 10 kips]

TABLE A.11

Strain Gauge Results and Derived Stresses

in Cartesian Coordinates

Position	$e_x \times 10^6$	$e_y \times 10^6$	$e_{xy} \times 10^6$	σ_x (psi)	σ_y (psi)	τ_{xy} (psi)
Value						
C.6	- 292	66	- 24	- 8816	- 224	- 290
C.7	- 368	112	- 53	-10880	640	- 673
D.6	- 275	94	12	- 8045	819	139
D.7	- 412	124	35	-12192	672	416
F.6	- 268	91	101	- 7851	757	1219
F.7	- 330	100	57	- 9859	525	679
H.6	- 255	79	100	- 7528	488	1206
H.7	- 255	82	66	- 7507	573	790
J.6	- 242	69	67	- 7195	261	804
J.7	- 174	55	65	- 5125	379	776
L.6	- 224	50	3	- 6768	- 192	42
L.7	- 135	45	14	- 3960	360	166
M.6	- 205	58	- 29	- 6093	227	- 346
M.7	- 193	52	- 21	- 5757	131	- 249

Test No. 4: P = 10 kips

TABLE A.12

Comparison of Experimental and Theoretical Results (σ_t)

	Experimental	Ring Theory	Small Hole Theory
H.1	- 17,300	- 14,100	- 14,700
I.1	- 17,890	- 14,100	- 15,900
J.1	- 19,335	- 14,100	- 18,000
K.1	- 20,950	- 14,100	- 20,700
L.1	- 9,840	- 9,700	- 15,200
M.1	5,820		2,750
N.1	11,365		7,500

Test No. 1: P = 40 kips

TABLE A.13

Comparison of Experimental and Theoretical Results (σ_t)

	Experimental	Ring Theory	Small Hole Theory	Combined Theory
B.1	15,050		12,200	
C.1	27,775		15,200	
D.1	32,735	27,700	10,000	26,700
E.1	24,950	21,100	2,000	20,000
F.1	13,250	14,500	- 1,100	13,500
G.1	4,470	6,000	- 2,500	5,700
H.1	- 3,800	- 2,400	- 3,200	- 2,400
I.1	-11,990	- 11,500	- 5,000	- 11,500
J.1	-21,175	- 19,700	- 7,900	- 20,500
K.1	-33,910	- 26,350	- 12,000	- 27,900
L.1	-38,400	- 30,900	- 17,500	- 32,000
M.1	-26,925		- 14,500	
N.1	-12,110		- 9,000	

Test No. 2: P = 10 kips

TABLE A.14

Comparison of Experimental and Theoretical Results (δ_t)

	Experimental	Ring Theory	Small Hole Theory	Combined Theory
B.1	12,045		8,000	
C.1	22,480		9,000	
D.1	24,160	20,550	3,500	19,000
E.1	16,185	15,000	- 2,000	13,250
F.1	7,430	9,500	- 3,100	8,400
G.1	960	2,500	- 3,900	1,900
H.1	- 5,610	- 4,100	- 4,500	- 4,100
I.1	- 12,380	- 11,000	- 5,200	- 11,000
J.1	- 20,700	- 17,500	- 7,100	- 18,500
K.1	- 29,850	- 22,800	- 9,600	- 25,000
L.1	- 32,485	- 26,000	- 12,000	- 27,500
M.1	- 20,750		- 9,600	
N.1	- 7,625		- 3,600	

Test No. 3: P = 10 kips

TABLE A.15

Comparison of Experimental and Theoretical Results (δ_t)

	Experimental	Ring Theory	Small Hole Theory	Combined Theory
B.1	10,600		6,800	
C.1	17,800		7,000	
D.1	16,500	14,100	1,300	12,400
E.1	9,780	9,790	- 3,800	8,000
F.1	3,780	5,100	- 4,500	4,500
G.1	- 1,350	0	- 1,500	0
H.1	- 6,540	- 5,000	- 4,900	- 4,800
I.1	- 11,400	- 9,800	- 5,500	- 9,800
J.1	- 16,860	- 14,500	- 7,200	- 16,000
K.1	- 25,140	- 19,000	- 9,600	- 21,000
L.1	- 26,200	21,000	- 10,600	- 22,200
M.1	- 15,600		- 5,900	
N.1	- 5,600		- 1,900	

Test No. 4: P = 10 kips

TABLE A.16

Deflections of the Beam (Inch)

Test No. 1

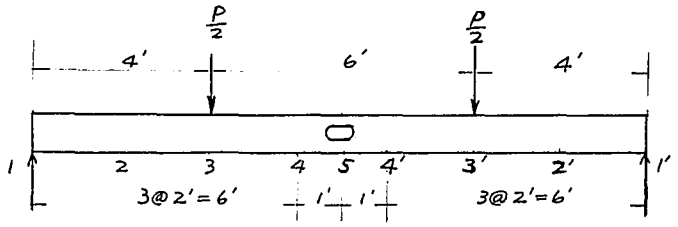

Measured Values

Point / Total Load (kips)	2	3	4	5	4'	3'	2'
10	0.040	0.071	0.086	0.092	0.089	0.075	0.044
20	0.080	0.146	0.177	0.181	0.178	0.146	0.085
30	0.120	0.220	0.267	0.242	0.269	0.221	0.126
40	0.160	0.293	0.365	0.361	0.360	0.292	0.163
50	0.201	0.366	0.442	0.451	0.447	0.367	0.206
60	0.244	0.453	0.531	0.542	0.537	0.450	0.249
70	0.300	0.549	0.663	0.651	0.678	0.550	0.305
Theoretical Values (gross section)							
20	0.083	0.150	0.182	0.186	0.182	0.150	0.083

Note: 1. The measured values have been corrected for the errors due to the yielding of supports.

2. Theoretical values were based on the gross section of the beam, with shear effect taken into consideration. The value of E was taken as 30×10^6 psi.

3. The theoretical values being slightly larger than the measured values may be explained by the following factors: non-homogeneity of the beam material; assumptions in the theory for calculating shear deflections; the value of E.

TABLE A.17

Deflections of the Beam (Inch)

Test No. 2

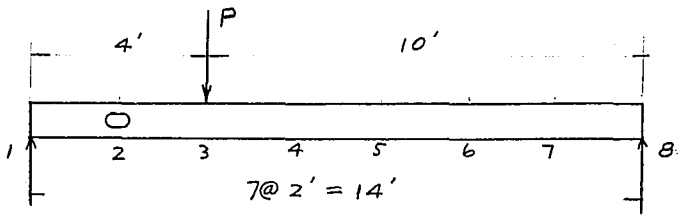

Measured Values

Point / Total Load (kips)	2	3	4	5	6	7
5	0.032	0.055	0.059	0.054	0.048	0.025
10	0.065	0.111	0.119	0.108	0.085	0.047
20	0.142	0.239	0.248	0.222	0.163	0.087
30	0.290	0.512	0.496	0.424	0.304	0.158
Theoretical Values (gross section)						
10	0.048	0.084	0.095	0.087	0.065	0.035

TABLE A.18

Deflections of the Beam (Inch)

Test No. 3

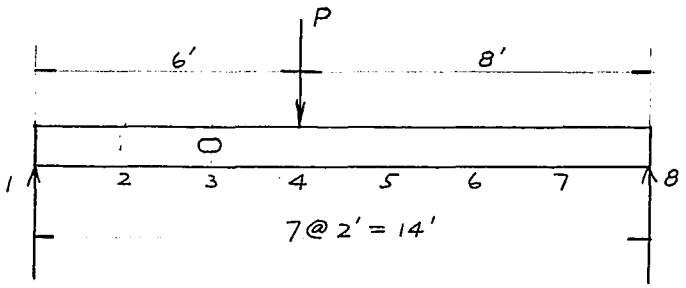

Measured Values

Point / Total Load (kips)	2	3	4	5	6	7
5	0.028	0.053	0.072	0.069	0.051	0.029
10	0.054	0.107	0.144	0.133	0.102	0.058
Theoretical Values (gross section)						
10	0.052	0.095	0.119	0.114	0.87	0.047

TABLE A.19

Deflections of the Beam (Inch)

Test No. 4

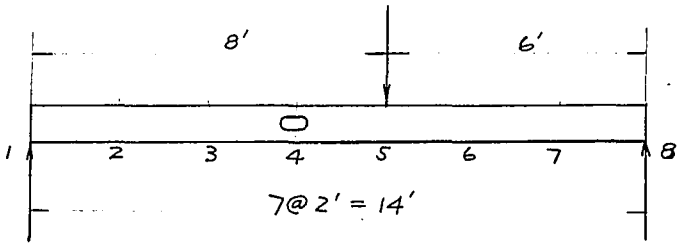

Measured Values

Point / Load (kips)	2	3	4	5	6	7
5	0.027	0.044	0.065	0.071	0.059	0.034
10	0.051	0.089	0.127	0.140	0.114	0.066

Theoretical Values (gross section)

10	0.047	0.087	0.114	0.119	0.095	0.052

APPENDIX B

SAMPLE CALCULATIONS

B.1 ELASTIC TANGENTIAL STRESSES AT THE BOUNDARY OF THE OPENING - COMBINED THEORY

Test No. 2 P = 10 kips

The tangential stresses at the boundary of opening can be calculated by superposition as shown in Figure B-1.

1. Stresses due to pure bending - small hole theory

By equation 2-1 the tangential stresses at points 1 and 2 (Figure B-2) are calculated as

$$(\sigma_t)_1' = -3{,}320 \text{ psi}$$

$$(\sigma_t)_2' = -3{,}100 \text{ psi}$$

The values shown are calculated by computer.

2. Stresses due to pure shear - ring theory

Point 1

The effective width of the flange is taken arbitrarily as 90% of its original width, then, from Figure B-2

$$(\sigma_t)_1'' = -\frac{3570 \times 3.39 \times 2.41}{1.528}$$

$$= -19{,}100 \text{ psi}$$

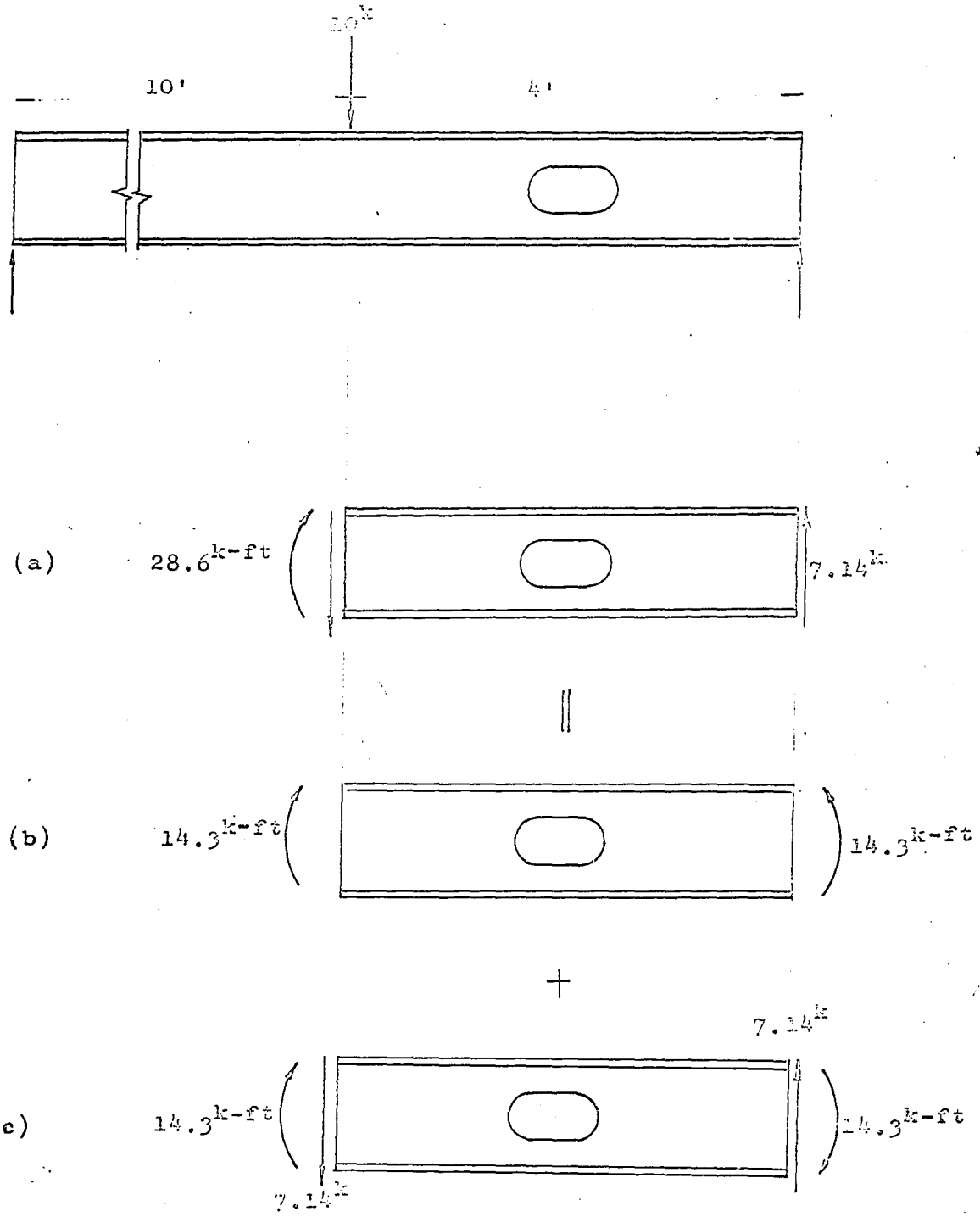
10k
10'
4'
(a)
28.6k-ft
7.14k
(b)
14.3k-ft
14.3k-ft
(c)
7.14k
14.3k-ft
14.3k-ft
7.14k

Fig. B-1

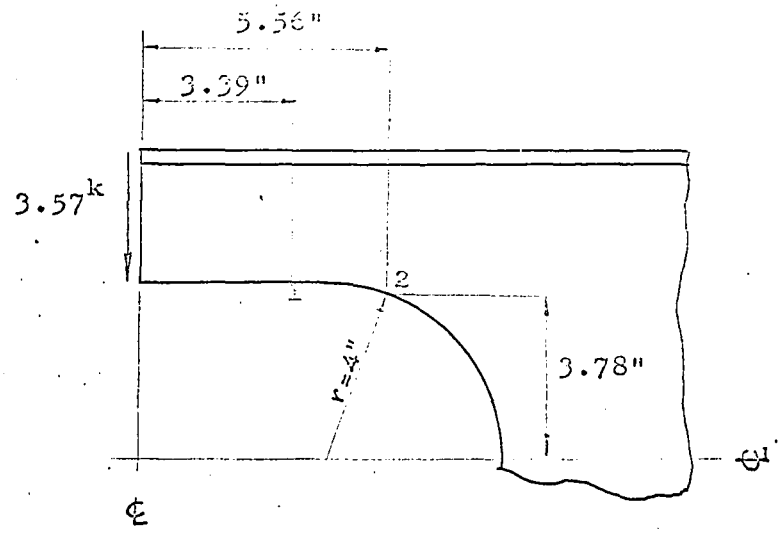

(a)

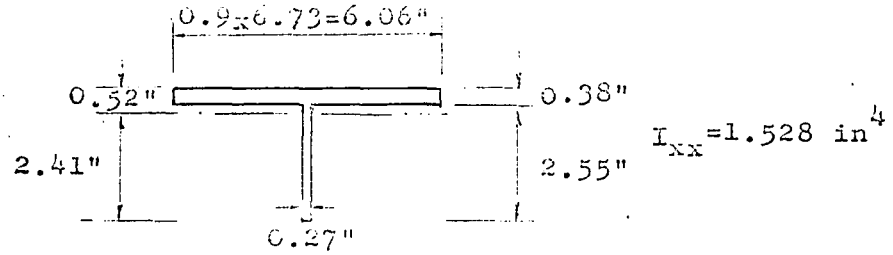

(b) Tee-section through Point 1.

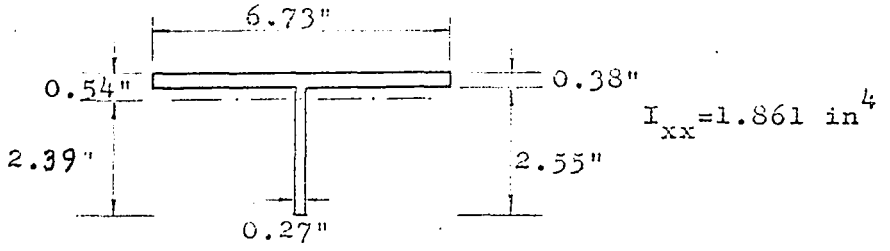

(c) Tee-section through Point 2.

Fig. B-2

Point 2

Similarly, from Figure B-2

$$[\sigma_t]_2'' = - \frac{3570 \times 5.56 \times 2.39}{1.867} \times \frac{4}{3.78}$$

$$= - 29{,}200 \text{ psi}$$

3. Total Stresses

$$[\sigma_t]_1 = - 3{,}320 - 19{,}100 = - 22{,}420 \text{ psi}$$

$$[\sigma_t]_2 = - 3{,}100 - 29{,}200 = - 32{,}300 \text{ psi}$$

B.2 ULTIMATE STRENGTH OF THE BEAM

Test No. 2

Refer to Figures 3-4

D = 2.55" a = 8.5" b = 6.73"

L = 24" h_c = 13" t_w = 0.27"

t_f = 0.38" $\sigma_{y.p.}$ = 51 ksi

$$\frac{a}{3} = \frac{8.5}{3} = 4.91 > 2.55$$

Therefore the beam will fail by a four hinge mechanism.

From equation 3-9 we obtain

$$\left(\frac{3}{4} + \frac{24^2}{13^2} + \frac{3 \times 6.73}{2 \times 0.38} \right) R^2 + 51 \times (8.5 \times 6.73 + 3 \times 6.73 \times 0.38$$

$$- 3 \times 2.55 \times 0.27) R + 51^2 \times [2.55^2 \times 0.27^2 - 6.73^2 \times 0.38^2$$

$$- 2 \times 6.73 \times 2.55 \times 0.27 \times (2.55 + 0.38)] = 0$$

i.e. $41.56R^2 + 51 \times 60.43R - 51^2 \times 33.21 = 0$

Solving the equation gives

$$R = 21.7 \text{ kips}$$

$$P = \frac{14}{10} \times 21.7 = 30.4 \text{ kips}$$

$$k_1 = \frac{0.38}{2} + \frac{2.55 \times 0.27}{2 \times 6.73} + \frac{24}{2 \times 13 \times 6.73 \times 51} - \frac{3}{4 \times 6.73 \times 51}$$

$$= 0.272 < 0.38$$

B.3 THEORETICAL DEFLECTION OF THE BEAM (GROSS SECTION)

Test No. 2 P = 10 kips $E = 30 \times 10^6$ $\mu_s = 0.25$ $I = 289.6 \text{ in}^4$

Point 4 (Figure B-3a)

1. Deflection due to bending moment

$$\Delta_4' = \frac{Pa_1(L - x_1)}{6EIL} (2Lx_1 - a_1^2 - x_1^2)$$

$$= \frac{10{,}000 \times 48 \ (168 - 72)}{6 \times 30 \times 10^6 \times 289.6 \times 168} (2 \times 168 \times 72 - 48^2 - 72^2)$$

$$= 0.0878"$$

2. Deflection due to shear[33]

V (shear force at point 4) = 2.86 kips

$$G = \frac{30 \times 10^6}{2(1 + 0.25)} = 12 \times 10^6 \text{ psi}$$

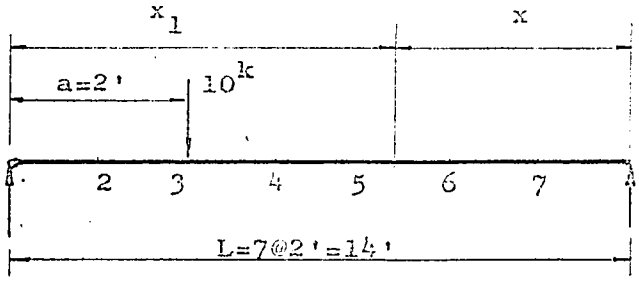

(a)

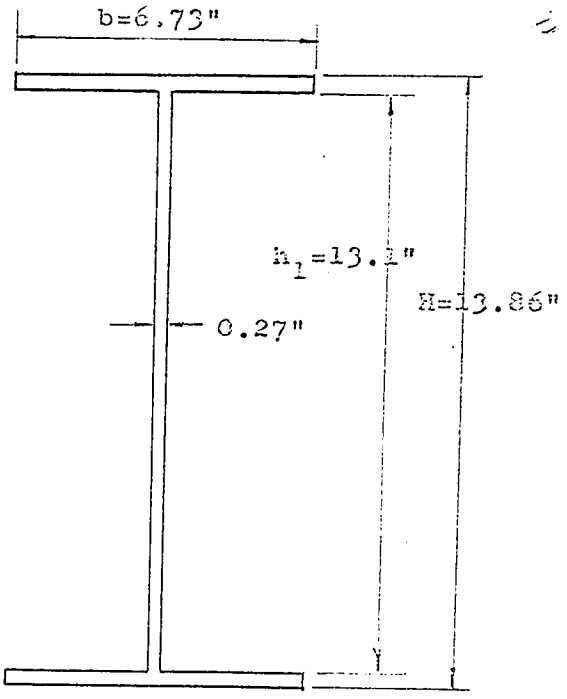

(b) Nominal Beam Dimensions.

Fig. B-3

$$\frac{k}{AG} = \frac{1}{t_w I}\left[\frac{bH^2}{8} - \frac{h_1^2}{8}(b - t_w)\right]$$

$$= \frac{1}{0.27 \times 289.6}\left[\frac{6.73 \times 13.86^2}{8} - \frac{13.1^2}{8}(6.73 - 0.27)\right]$$

$$= 0.297$$

$$\Delta_4'' = \frac{kV}{AG} x$$

$$= \frac{2860 \times 0.297}{12 \times 10^6} \times 8 \times 12$$

$$= 0.0068"$$

3. Total Deflection

$$\Delta_4 = 0.0878 + 0.0068$$

$$= 0.0946$$

$$= 0.095"$$

APPENDIX C

REINFORCEMENT CORRECTION FACTOR (F_c)*

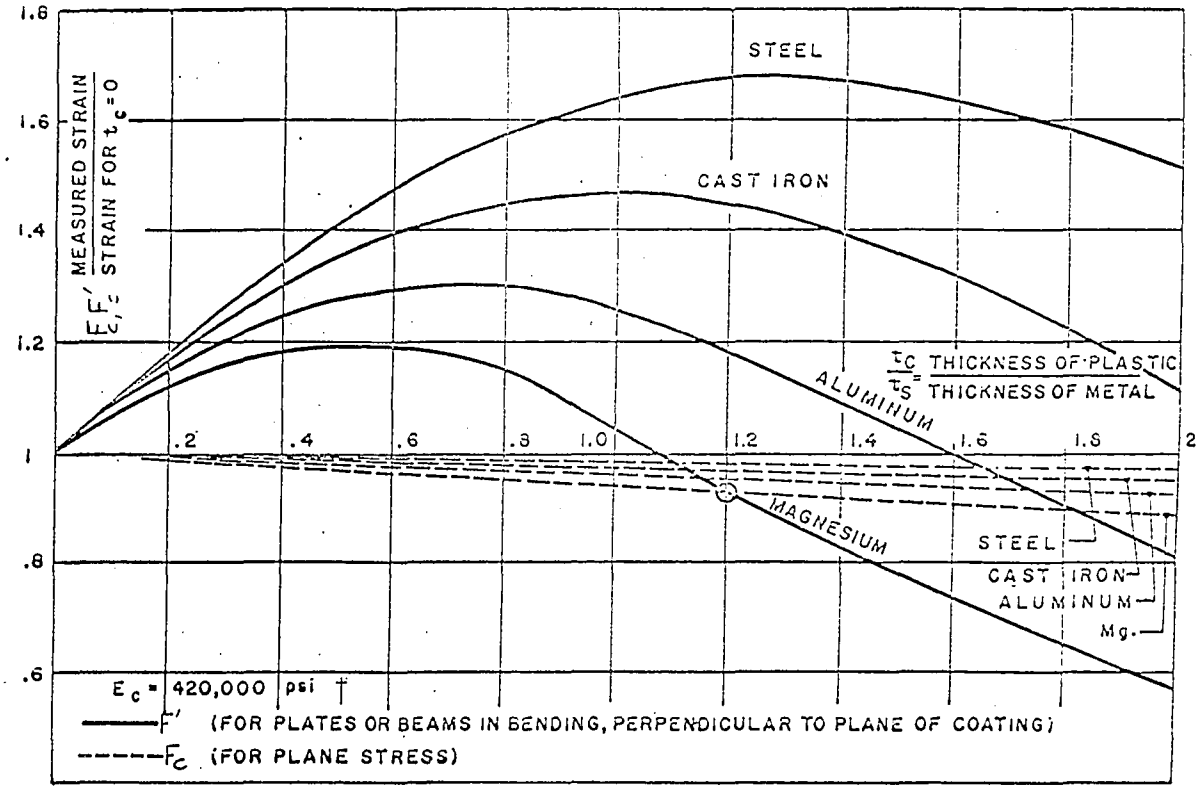

* This chart is due to Zandman et al[34]

† E_c is the Young modulus of the Plastic sheet

APPENDIX D

TABLE D.1

Coefficients of Mapping Function*

$K = \frac{2r}{a + 2r}$	A	B	C	D	E
1/4	0.33546	0.18773	- 0.02473	+ 0.00002	+ 0.00177
2/7	0.34499	0.17788	- 0.02533	+ 0.00122	+ 0.00116
1/3	0.35730	0.16482	- 0.02550	+ 0.00279	+ 0.00153
2/5	0.37391	0.14668	- 0.02469	+ 0.00490	+ 0.00078
1/2	0.39776	0.11997	- 0.02148	+ 0.00730	- 0.00128
2/3	0.43522	0.07581	- 0.01733	+ 0.00837	- 0.00256
1.0	0.5	0	0	0	0

* From the results by Heller et al.[23]

BIBLIOGRAPHY

1. Kirsch, G. "Die Theorie Der Elastisitätud Die Bedürfnisse Der Festigkeitslehre", Zeitschrift Des Vereines Deutscher Ingenieure, Vol. 42, 1898.
2. Tuzi, Z. "Effect of a Circular Holes on Stress Distribution of a Beam under Uniform Bending Moment", Scientific Papers of Tokyo Institute of Physical and Chemical Research, Vol. 9, Aug. 20, 1928, pp. 65-89.
3. Timoshenko, S. and Goodier, J.N. "Theory of Elasticity", 2nd. Edition. McGraw-Hill Book Co., New York, 1951, p.81.
4. Howland, R.C.J. and Stevenson, A.C. "Biharmonic Analysis in a Perforated Strip", Philosophical Transactions of the Royal Society of London, Series A, Vol. 233, 1933, pp. 155-222.
5. Knight, R.C. "On the Stresses in a Perforated Strip", Quarterly Journal of Mathematics, Oxford Series, Vol. 5, 1934, pp. 255-268.
6. Hengst, H. "Beitrag zur Beurteilung des Spannungszustandes einer gelochten Scheibe" Zeitschrift für Angewandte Mathematik und Mechanik, Vol. 18, Feb. 1938, pp. 44-48.
7. Wang, C.K. "Theoretical Analysis of Perforated Shear Web", ASME Transactions, Journal of Applied Mechanics, 1946, p.A-77.
8. Ling, C.B. "Stresses in a Perforated Strip", ASME Transactions, Journal of Applied Mechanics, 1957, pp. 365-375.

9. Gibson, J.E. and Jenkins, W.M. "Stress Distribution in Simply Supported Beam with Circular Hole", Structural Engineering, Dec. 1956.

10. So, W.C. "The Stresses Around Large Circular Openings in the Webs of Wide-Flange Beam", M.Eng. Thesis, McGill University, Aug. 1963.

11. Kolosoff, G. Doctoral Dissertation, Dorpat, 1909. see Reference 3, p. 198.

12. Inglis, C.E. "Stresses in a Plate due to the Presence of Cracks and Sharp Corners", Transactions of the Institution of Naval Architects, Vol. 55, London, 1913, pp. 219-242.

13. Wolf, K. "Beiträge zur ebenen Elastizitätstheorie", Zeitschrift für technische Physik, Vol. 2, No.8, 1921, pp. 209 and Vol. 3, No. 5, 1922, pp. 160-166.

14. Neuber, H. "Kerbspannungslehre", Springer, Berlin, 1937. Translation, "Theory of Notch Stresses", J.W. Edwards Co., Ann Arbor, Mich., 1946.

15. Greenspan, M. "Effect of a Small Hole on the Stresses in a Uniformly Loaded Plate", Quarterly Applied Mathematics, Vol. 2, 1944, pp. 60-71.

16. Green, A.E. "Stress Systems in Isotropic Aelotropic Plates" Proceedings, Royal Society of London, Series A, Vol. 184, 1945, pp. 231.

17. Muskhelishvili, N.I. "Some Basic Problems of the Mathematical Theory of Elasticity", 2nd Edition, P. Noordhoff Ltd. 1963.

18. Morkovin, V. Discussion of "Effect of a Small Hole on the Stresses in a Uniformly Loaded Plate", Quarterly Applied Mathematics, Vol. 2, No. 4, 1944, pp. 350-352.

19. Savin, G.N. "Stress Concentration Around Holes", Pergamon Press, 1961.

20. Joseph, J.A. and Brock, J.S. "The Stresses Around a Small Opening in a Beam Subjected to Pure Bending", ASME Transactions, Journal of Applied Mechanics, Vol. 72, Dec. 1950, pp. 353-358.

21. Heller, S.R. Jr. "The Stresses Around a Small Opening in a Beam Subjected to Bending with Shear", Proceedings of the 1st U.S. National Congress of Applied Mechanics, ASME, New York, 1951, pp. 239-245.

22. Heller, S.R. Jr., Brock, J.S. and Bart, R. "The Stresses Around a Rectangular Opening with Rounded Corners in a Uniformly Loaded Plate", Proceedings of the Third U.S. National Congress of Applied Mechanics, 1958, pp. 357-368.

23. Heller, S.R. Jr., Brock, J.S. and Bart, R. "The Stresses Around a Rectangular Opening with Rounded Corners in a Beam Subjected to Bending with Shear", Research and Development Report 1311, David Taylor Model Basin, Washington, D.C. 1959.

24. Bower, J.E. "Elastic Stress Around Holes in Wide-Flange Beam" Journal of Structural Division, ASCE, Vol. 92, No. ST2, April 1966.

25. Blodgett, O.M. "The Application and Design of Cost-Saving Open-Web Expended Beam and Girders", Lincoln Electric Company Studies in Structural Arc Welding Bulletin 1302,199.

26. Segner, E.P. Jr. "An Investigation of the Requirements for Reinforcement Around Large Rectangular Openings in the Webs of Wide-Flange Beams, Subjected to Bending Moment and Shear", Texas Engineering Experiment Station Report No. E-81-62, College Station, Texas, January 1963.

27. McClellan, T.J. "Effects of Openings in Webs of Steel Girders", presented at the Structural Engineers Association of California Convention, October 2, 1964.

28. Bower, J.E. "Experimental Elastic Stresses in Wide-Flange Beams with Web Holes", presented at the joint ASCE - CICM Structural Engineering Meeting, Mexico City, February 7, 1966.

29. Worley, W.J. "Inelastic Behaviour of Aluminum Alloy I-Beams with Web Cutouts", University of Illinois Engineering Experiment Station, Bulletin No. 448.

30. Bower, J.E. "Ultimate Strength of Wide-Flange Beams with Rectangular Web Holes", Unpublished report to United Steel Corporation.

31. Budd Instrument Ltd. "Instruction Manual for the Photostress Large Field Meter and its Accessories Model LF/MU" Instruments Division of the Budd Company, p.16.

32. See Reference 3, p. 172.

33. Timoshenko, S. and MacCullough, G.H. "Elements of Strength of Materials", 3rd Edition, D. Van Nostrand Company, New York, p. 196.

34. Zandman, F., Redner, S.S. and Riegner, E.I. "Reinforcing Effect of Birefringent Coatings", Experimental Mechanics, SESA, February 1962.